https://doi.org/10.5194/egusphere-2026-3647
Preprint. Discussion started: 8 July 2026

First field deployment of VIA-NO_3-CIMS for molecular characterization and source apportionment of particle-phase oxygenated organic molecules in eastern China

Maoyu Cao[1], Chao Yan[1,2,*], Yuliang Liu[1], Dafeng Ge[1], Junchao Yin[1], Yuanyuan Li[3], Tao Xu[2], Ziqian Wei[2], Jinbo Wang[4], Ying Zhang[1], Zhenning Wang[1], Valter Mickwitz[3], Ziheng Chen[1], Bisen Han[2], Jianxun Wang[2], Caijun Zhu[1], Ximeng Qi[2], Qiaozhi Zha[1], Xuguang Chi[1], Zhe Wang[5], Jian Zhao[3], Mikael Ehn[3], Wei Nie[1,2], Jingkun Jiang[6], Aijun Ding[1,2]

[1]School of Atmospheric Sciences, Nanjing University, Nanjing, 210046, China

[2]Nanjing-Helsinki Institute in Atmospheric and Earth System Sciences, Nanjing University, Suzhou, 215163, China

[3]Institute for Atmospheric and Earth System Research/Physics, Faculty of Science, University of Helsinki, Helsinki, 00014, Finland

[4]National Satellite Meteorological Center (National Center for Space Weather), China Meteorological Administration, Beijing, 100081, China

[5]Division of Environment and Sustainability, The Hong Kong University of Science and Technology, Hong Kong SAR, 999077, China

[6]State Key Joint Laboratory of Environment Simulation and Pollution Control, School of Environment, Tsinghua University, 100084 Beijing, China

Correspondence: Chao Yan (chaoyan@nju.edu.cn)

Abstract

Secondary organic aerosol (SOA) is a major component of fine particulate matter, yet its molecular-level characterization remains challenging. Here, we systematically evaluated the performance of a Volatilization Inlet for Aerosols coupled with nitrate chemical ionization mass spectrometry (VIA-NO_3-CIMS), including particle transmission, volatilization behavior, quantitative response, and operational stability. Following instrument characterization, the first field deployment of VIA-NO_3-CIMS was conducted at the SORPES station in Nanjing, eastern China. A high-confidence dataset containing 1,695 particle-phase oxygenated organic molecules (OOMs) was established. The summed OOM concentration correlated strongly with AMS-derived organic aerosol concentrations ($r = 0.88$), demonstrating the quantitative capability of VIA–NO_3–CIMS. Compared with gas-phase species, particle-phase OOMs exhibited larger carbon numbers, higher unsaturation, and lower volatility, with low-volatility compounds dominating the particle phase. Positive matrix factorization resolved seven SOA factors, including three biogenic-dominated, two anthropogenic-dominated, one regional background, and one pollution-episode factor. These factors contributed approximately 36.5%, 35.4%, 15.6%, and 12.1% of the total particle-phase OOM signal, respectively. Their molecular characteristics and temporal behaviors indicate important influences from daytime photochemistry, nighttime NO_3 oxidation, regional transport, and episodic pollution accumulation. Factor contributions evolved systematically with $PM_{2.5}$, with freshly formed SOA dominating under clean conditions and the pollution-episode factor becoming increasingly important as pollution levels increased, eventually dominating under the most polluted conditions. These results demonstrate that VIA-NO_3-CIMS enables quantitative molecular-level characterization and source apportionment of particle-phase SOA, providing new insights into the composition and evolution of urban organic aerosols.

1、Introduction

Organic aerosol (OA) exerts profound impacts on air quality, human health, and climate by perturbing Earth’s radiative balance and cloud microphysics (Jimenez et al., 2009; Lelieveld et al., 2015; Shrivastava et al., 2017). In urban China, secondary organic

https://doi.org/10.5194/egusphere-2026-3647
Preprint. Discussion started: 8 July 2026

aerosol (SOA) has increasingly emerged as the dominant OA component over the past decade, with formation governed by region-specific chemistry (Hallquist et al., 2009; Huang et al., 2014; Huang et al., 2025). SOA formation involves coupled multi-phase processes: gas-phase oxidation by OH, O_3, and NO_3 produces low-volatility products that partition into the particle phase, and condensed-phase reactions—including aqueous and acid-catalyzed chemistry, accretion, and oligomerization—further modify composition, oxidation state, and volatility (Jang et al., 2002; Kroll & Seinfeld, 2008; Zhang et al., 2015; Kenseth et al., 2023). The relative importance of these pathways depends on volatile organic compound (VOC) precursor identity, oxidant concentrations, aerosol liquid water content, particle acidity, and NOx levels, leading to substantial spatiotemporal variability in source attribution and formation pathways (Ng et al., 2007; Zhao et al., 2018; Pye et al., 2020).

Over the past two decades, the high-resolution time-of-flight aerosol mass spectrometer (HR-ToF-AMS, hereafter AMS) has been widely used to study OA (DeCarlo et al., 2006; Canagaratna et al., 2007; Jimenez et al., 2009; Lee et al., 2013). The electron impact ionization at 70eV allows for complete ionization of non-refractory PM_1 (NR-PM_1), and thus AMS can provide an accurate quantification of OA. Positive matrix factorization (PMF) applied to AMS measurements typically resolves several environmentally meaningful OA factors, including hydrocarbon-like OA (HOA), cooking OA (COA), biomass burning OA (BBOA), and oxygenated OA (OOA), the latter often further separated into less oxidized (LO-OOA) and more oxidized (MO-OOA) components (Sun et al., 2013; Wang et al., 2016). However, because AMS relies on electron-impact (EI) ionization, extensive molecular fragmentation occurs, and the resulting factors mainly reflect bulk chemical properties rather than molecular-level composition. Consequently, these factors can describe average oxidation state and volatility, but are generally not source-specific or process-specific. This limitation remains a major obstacle toward process-level understanding of SOA formation.

To overcome this limitation, a suite of molecular-level mass spectrometric techniques has been developed to provide enhanced chemical resolution of aerosol speciation (Li et al., 2023; Sun et al., 2025). The Filter Inlet for Gases and AEROsols (FIGAERO) coupled with Iodide chemical ionization mass spectrometry (I-CIMS) has been widely applied to probe SOA volatility distributions and composition by sequentially thermally desorbing filter-collected particles (Lopez-Hilfiker et al., 2014; Buchholz et al., 2020; Voliotis et al., 2021). This approach provides valuable molecular information, although its time resolution is constrained by filter collection and desorption cycles, and thermal decomposition or interfacial reactions may influence observed signals (Stark et al., 2017; Yang et al., 2021). Extractive electrospray ionization mass spectrometry (EESI-MS) provides near-real-time detection of particle-phase constituents without requiring particle collection and thermal desorption steps (Lopez-Hilfiker et al., 2019; Lee et al., 2022). While EESI-MS offers high time resolution and minimizes thermal artifacts, ionization selectivity, matrix effects, high background signal, and quantitative calibration remain challenging. Notably, these techniques rely on different reagent ions and ionization mechanisms, which inherently affect molecular selectivity and sensitivity. Consequently, intercomparison among particle-phase molecular measurement methods, as well as consistency between particle- and gas-phase oxygenated organic molecules (OOMs) composition, remains challenging.

A recent development is the Volatilization Inlet for Aerosols (VIA) coupled with nitrate chemical ionization mass spectrometry (NO_3-CIMS), in which submicron particles can be volatilized in real time and ionized by NO_3^- reagent ions in prior to mass spectrometric detection (Häkkinen et al., 2023; Zhao et al., 2024). By employing controlled heating and a short residence time (~0.1 s), VIA minimizes thermal-desorption artifacts and secondary decomposition during volatilization (Häkkinen et al., 2023; Zhao et al., 2024). More importantly, this system uses the same nitrate reagent ion (NO_3^-) to detect OOMs in the particle phase, enabling direct comparison with gas-phase OOMs widely measured by nitrate CIMS (Liu et al., 2021; Nie et al., 2022; Liu et al., 2023; Yuan et al., 2024; Yin et al., 2025). By eliminating systematic biases associated with different ionization schemes, this approach provides a unified molecular framework for investigating gas–particle partitioning and compositional

https://doi.org/10.5194/egusphere-2026-3647
Preprint. Discussion started: 8 July 2026

differences. Such capability is critical for identifying authentic phase-dependent chemical signatures and for constraining the processes governing SOA formation, aging, and phase evolution.

In this study, we present the first field deployment of VIA-NO_3-CIMS in Nanjing, eastern China, alongside parallel HR-ToF-AMS measurements, to investigate the molecular composition, gas–particle partitioning behavior, and source contributions of particle-phase OOMs. Prior to field application, key performance characteristics—including particle transmission efficiency, volatilization behavior, and quantitative response—were systematically evaluated to ensure reliable molecular-level observations under ambient conditions. Using this validated system, the molecular composition and chemical characteristics of particle-phase OOM were comprehensively characterized and compared with their gas-phase counterparts, revealing distinct molecular signatures associated with gas–particle partitioning and atmospheric aging. Molecular-level source apportionment using PMF further resolved multiple SOA factors associated with biogenic, anthropogenic, and regionally aged sources. These findings demonstrate that VIA-NO_3-CIMS enables robust molecular-level characterization of particle-phase organics, providing a chemically resolved framework for understanding SOA sources, formation pathways, and atmospheric evolution in urban environments.

2、Method

2.1 Sampling site

Field observations were conducted from 17 September to 11 October 2024 at the Station for Observing Regional Processes of the Earth System (SORPES; 32°07′14″ N, 118°57′10″ E) at Xianlin Campus of Nanjing University. This station is ~20 km northeast to the downtown Nanjing and commonly considered as a sub-urban station. The site sits on a small, vegetation-covered hill and is directly influenced by local biogenic emissions. Depending on meteorological conditions, the site can also be intermittently affected by urban air masses transported from downtown Nanjing. This location, situated at the interface between urban and vegetated environments, provides an ideal platform for investigating secondary organic aerosol formation influenced by both anthropogenic and biogenic precursors. Detailed descriptions of the station are available in previous studies (Nie et al., 2015; Ding et al., 2016; Liu et al., 2021).

2.2 Instrumentation

2.2.1 VIA-NO_3-CIMS

An online Volatilization Inlet for Aerosols (VIA) coupled with a nitrate chemical ionization mass spectrometer (NO_3-CIMS) was used to measure OOMs in the particle phase. As illustrated in Fig. 1, the core components of the VIA-NO_3-CIMS system include a background-switching module, a gas-phase denuder, an evaporation tube, a sheath-flow unit, and a NO_3-CIMS.

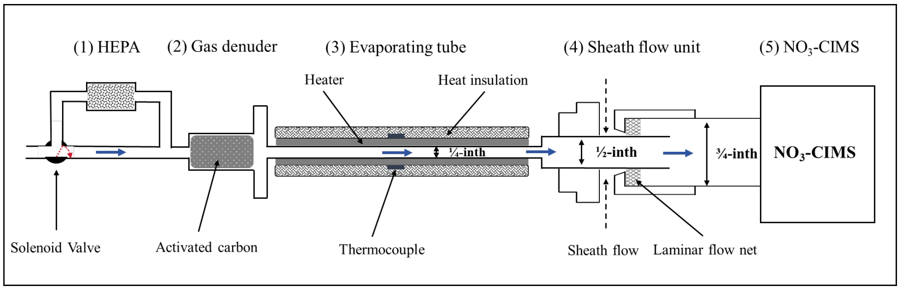

Figure 1. Schematic of the experimental setup, comprising (1) Particle and background switching unit, (2) a gas-phase denuder, (3) a vaporization tube, (4) a sheath flow unit, and (5) a NO_3-CIMS. The blue arrows indicate the sampling flow direction. Note that the figure is not drawn to scale.

At the upstream end of the sampling line, a high-efficiency particulate air (HEPA) filter was installed in parallel and switched into the main sampling stream every 10 minutes via a solenoid valve to enable automated background measurements. The aerosol flow then passed through a ~4 cm honeycomb activated carbon denuder to remove interfering gas-phase species. Reported performance for such denuders is 97–99.9 % VOC removal with > 90 % transmission for particles > 50 nm (Häkkinen et al., 2023; Zhao et al., 2024). Downstream of the denuder, the aerosol entered a 40 cm-long, ¼ inch i.d. Sulfinert®-coated stainless-steel heating tube, externally wrapped with a heating tape and insulated with glass wool. Measurements using ambient aerosol particles showed that the total particle-phase OA signal increased with temperature and reached a maximum at 300 °C (Fig. S1a). Therefore, 300 °C was selected as the operating temperature for all subsequent field measurements. To quantitatively assess the volatilization efficiency under the operating conditions used here, size-selected ambient aerosol particles were introduced into the VIA and particle volume loss upon heating to 300 °C was evaluated using SMPS measurements. These experiments indicate that, on average, approximately 70 % of particle-phase organic material was volatilized, with weak size dependence across the investigated diameter range (50–470 nm; Fig. S2). Accordingly, VIA-derived particle-phase organic signals are interpreted as representing the volatilized fraction of condensed-phase oxygenated organics under these optimized conditions. The resulting vapor flow immediately entered a 5 cm cooling tube, and was merged coaxially into a 45 cm transfer line directed toward the ion source. A 6 L min^{-1} flow of N_2 was introduced at this point to facilitate rapid cooling, suppress condensation and thermophoretic losses, and meet the high total flow requirements of the NO_3-CIMS system.

Detection was performed using an Atmospheric Pressure interface Time-of-Flight (APi-ToF) mass spectrometer coupled to an Eisele-type NO_3^- chemical ionization source (Aerodyne Research Inc. and Tofwerk AG). The sampling flow was set to 8.7 L min^{-1}, with an additional 25.5 L min^{-1} sheath flow introduced at the ion source to minimize wall losses. In the X-ray ionizer region, NO_3^- ions generated from HNO_3 clustered with or abstracted a proton from the evaporated neutral molecules, forming $[M\cdot NO_3]^-$ or $[M-H]^-$ ions that were subsequently detected by the ToF analyzer. The fundamental principles of the NO_3-CIMS technique have been described in detail in previous studies (Junninen et al., 2010; Jokinen et al., 2012). A more detailed discussion of the characterization and operating conditions of the VIA–NO_3–CIMS system is provided in Supplementary Information Sect. S1.

2.2.2 HR-ToF-AMS

A high-resolution time-of-flight aerosol mass spectrometer (HR-ToF-AMS; Aerodyne Research Inc.) equipped with a PM_1 aerodynamic lens was deployed at SORPES to quantify the chemical composition of non-refractory submicron particulate matter (NR-PM_1)—namely organic aerosol (OA), nitrate (NO_3^-), sulfate (SO_4^{2-}), ammonium (NH_4^+), and chloride (Cl^-). Ambient air was drawn through a ~2 m stainless-steel inlet, dried by a Nafion tube (relative humidity < 40 %), and passed through a 100 µm critical orifice into the aerodynamic lens, which focuses particles with vacuum-aerodynamic diameters of ~35–1000 nm into a narrow beam. After size characterization in the particle time-of-flight (PToF) region, particles impinged on a ~600 °C tungsten vaporiser and were flash-vaporised. The vapours were ionised by 70 eV electron impact and analysed in V-mode ($m/\Delta m \approx 2000–3000$) at 2 min time resolution. Instrument response was calibrated with size-selected 300 nm ammonium nitrate to determine the ionisation efficiency (IE). Default relative ionisation efficiencies (RIEs) of 1.4 (OA), 1.1 (NO_3^-), 1.3 (SO_4^{2-}), 4.5 (NH_4^+), and 1.3 (Cl^-) were applied, and a constant collection efficiency (CE) of 0.5, typical for ambient conditions, was assumed. Data were acquired with TofDAQ and processed using SQUIRREL v1.60P and PIKA v1.20P in Igor Pro 8.04.

2.2.3 Others instrumentation

A Vocus CI-ToF (Tofwerk AG) was deployed for high-time-resolution monitoring of VOCs. Meteorological parameters—air temperature, relative humidity, wind speed and direction, and surface pressure—were obtained from the SORPES automatic weather station. Since on-site gas measurements were not available during the observation period, the concentrations of $PM_{2.5}$, NO_2, and O_3 were obtained from the "Xianlin University Town" site, located approximately 2 km from SORPES (straight-line distance), and downloaded from the National Urban Air Quality Real-time Publishing Platform maintained by the China National Environmental Monitoring Center (https://air.cnemc.cn:18007/). A comparison of trace gas concentrations between the two sites were conducted using an overlapping period. The two datasets showed high correlations (r = 0.81–0.91) (Fig. S3), indicating that the substituted dataset is representative. Aerosol liquid water content (ALWC) was calculated with the ISORROPIA II thermodynamic equilibrium model. This comprehensive, high-resolution observational dataset provides a robust basis for investigating the chemical composition, sources, and transformation processes of atmospheric aerosols.

2.3 Source apportionment methods

To investigate the sources and chemical characteristics of OA, PMF analysis was independently performed on the high-resolution AMS mass spectra and the molecular-level VIA-NO_3-CIMS measurements. Positive matrix factorization (PMF) serves as the underlying receptor model. It decomposes complex mixtures into interpretable factors on the basis of their temporal and compositional variability, without requiring prior source profiles (Paatero & Tapper, 1994). Separate PMF analyses were conducted for the AMS and VIA-NO3-CIMS datasets using the multilinear engine ME-2 implemented in Source Finder (SoFi v6.8) (Canonaco et al., 2013). The ME-2 framework further allows the incorporation of a priori constraints—such as tracer signatures or known temporal patterns—thereby enhancing the robustness and interpretability of the resolved factors.

Mathematically, the observed data matrix X is approximated as:

$$X_{m\times n} = TS_{m\times p} \times MS_{p\times n} + E_{m\times n} \quad (1)$$

where TS represents the time series of the factors, MS denotes their spectral profiles, and E is the residual matrix. To account for measurement uncertainty, a weighted cost function Q is defined as:

$$Q = \sum_{i=1}^{m}\sum_{j=1}^{n}\left(\frac{E_{ij}}{S_{ij}}\right)^2 \quad (2)$$

The solution quality is assessed by comparing Q to its theoretical value Qexp, given by:

$$Q_{exp} = m \times n - p \times (m + n) \quad (3)$$

A good model fit is indicated when Q/Qexp approaches 1 and residuals are randomly distributed. The optimal number of factors was determined based on a combination of statistical diagnostics (e.g., Q/Qexp and residual distributions) and the interpretability and physical meaningfulness of the resolved factors.

2.4 The establishment of the oxygenated organic molecules dataset

2.4.1 Identification of oxygenated organic molecules

During this campaign, background and sample spectra were acquired in alternating 10-min cycles. Raw mass spectral data were first averaged to 10-min time resolution using tofTools (Junninen et al., 2010). Mass calibration was then applied to the entire dataset to ensure accurate mass assignment and consistent peak alignment across all spectra. Following mass calibration, background spectra obtained during HEPA-filter sampling periods were subtracted from the corresponding sample spectra to isolate particle-phase signals and remove residual gas-phase and instrumental background contributions. To robustly identify chemically meaningful peaks in the high-resolution mass spectra and to construct the OOM dataset, the bin-PMF approach was applied (Zhang et al., 2019). In this method, mass spectral signals were first linearly interpolated onto a uniform m/z grid with a resolution of 0.001 Th. For each nominal integer mass, signals were subsequently re-binned within a −0.25 to +0.45 Th window using a bin width of 0.004 Th. Only regions containing valid signal were retained, thereby excluding noise-dominated or empty m/z regions. This procedure resulted in approximately 175 bins per nominal mass interval, substantially reducing data dimensionality while preserving high-resolution spectral structure.

Based on this processing, a bin × time data matrix and its corresponding uncertainty matrix were constructed and used as input for PMF analysis without a priori constraints. High-resolution peak fitting was subsequently performed on the PMF factor profiles using tofTools to assign molecular formulas and resolve individual spectral features. Peaks that consistently appeared across multiple factors and exhibited stable signal characteristics were identified as high-confidence molecular features. These features were then used to reconstruct a robust particle-phase OOM dataset for subsequent molecular characterization, source apportionment, and quantitative analysis. Detailed descriptions of data processing procedures, matrix construction, and PMF configuration are provided in Supplementary Information Sect. S3.

2.4.2 Quantification of oxygenated organic molecules

To enable quantitative interpretation of the VIA-NO_3-CIMS measurements, instrument signals were first normalized to the total reagent ion signal. The concentration of each OOM was calculated as:

$$[OOM_i]_{molec} = ln(1 + \frac{\sum_{n=0}^{1}[OOM_i \cdot (HNO_3)_n \cdot NO_3^- + (OOM_i - H)^-]}{\sum_{n=0}^{2}[(HNO_3)_n \cdot NO_3^-]}) \cdot C \quad (4)$$

The numerator includes both the nitrate-adduct channels $OOM_i \cdot (HNO_3)_n \cdot NO_3^-$ (n=0,1) and the deprotonated channel $(OOM_i - H)^-$, the denominator represents the total nitrate reagent ion signal, and *C* denotes the calibration coefficient.

The corresponding mass concentration was then obtained by:

$$[OOM_i]_{\mu g/m^3} = [OOM_i]_{molec} \times \frac{MW}{N_A} \times 10^{12} \qquad (5)$$

where MW is the molecular weight (g mol^{-1}) and N_A is Avogadro's number.

Following conventional approaches, the calibration coefficient C was determined using sulfuric acid. Specifically, the normalized sulfuric acid signal measured by VIA-NO_3-CIMS was compared with particulate sulfate concentrations measured by AMS. A strong correlation was observed (r = 0.88; Fig. S7a), and linear regression (forced through the origin) yielded a slope of 5.99 μg m^{-3} per normalized signal unit,

https://doi.org/10.5194/egusphere-2026-3647
Preprint. Discussion started: 8 July 2026

corresponding to 3.68×10^{10} molecules cm^{-3}.

Applying this calibration, the summed particle-phase OOM signal accounted, on average, for approximately 22% of the SOA measured by AMS (Fig. S7b). This relatively low apparent mass fraction primarily reflects the intrinsic selectivity of nitrate chemical ionization, which preferentially detects highly oxygenated, low-volatility organic compounds, while exhibiting reduced sensitivity toward less oxidized or semi-volatile species. Furthermore, due to the fixed desorption temperature used in the VIA operation, while individual compounds may exhibit different Tmax values, some species may not be fully desorbed, potentially leading to an underestimation of their concentrations. Furthermore, we cannot exclude the possibility of thermal decomposition during the desorption process. While this effect is generally considered limited under the current operating conditions, its presence may still contribute to an underestimation of more volatile and thermally labile compounds.

Consequently, VIA-NO_3-CIMS quantifies a chemically specific subset of SOA, and the derived contribution should be interpreted as a conservative lower-bound estimate of particle-phase organic mass detectable by this technique. Nevertheless, a strong correlation was observed between total OOM mass concentration and SOA concentration ($r = 0.88$; Fig. S7c), indicating that VIA-NO_3-CIMS effectively captures the temporal variability of major SOA sources.

3 Results and discussion

3.1 Campaign overview and OA bulk properties

During the observation period, meteorological conditions and trace gas concentrations reflected characteristics typical of the late-summer to early-autumn transition in eastern China (Fig. 2a–c). The mean temperature was 21 ± 4 °C and relative humidity 68 ± 15 %, with synchronous increases during several high-humidity episodes. Wind speeds were generally below 3 m s^{-1}, with occasional peaks up to ~4 m s^{-1}, and wind directions shifted frequently between southerly and northerly sectors, indicating variable air-mass origins. Daytime O_3 concentrations increased markedly due to photochemical production, averaging 37.5 ± 21 ppb with peaks up to 105 ppb, whereas NO_2 exhibited multiple nighttime and early-morning maxima, with a campaign-average concentration of 11.9 ± 7.47 ppb. Overall, O_3 and NO_2 were negatively correlated ($r \approx -0.46$), reflecting active photochemical processing. Daytime NO_2 depletion was associated with enhanced boundary-layer mixing and photochemical oxidation, while nighttime O_3 depletion primarily resulted from titration by freshly emitted NO under shallow boundary-layer conditions. These conditions indicate an active photochemical environment conducive to secondary organic aerosol formation.

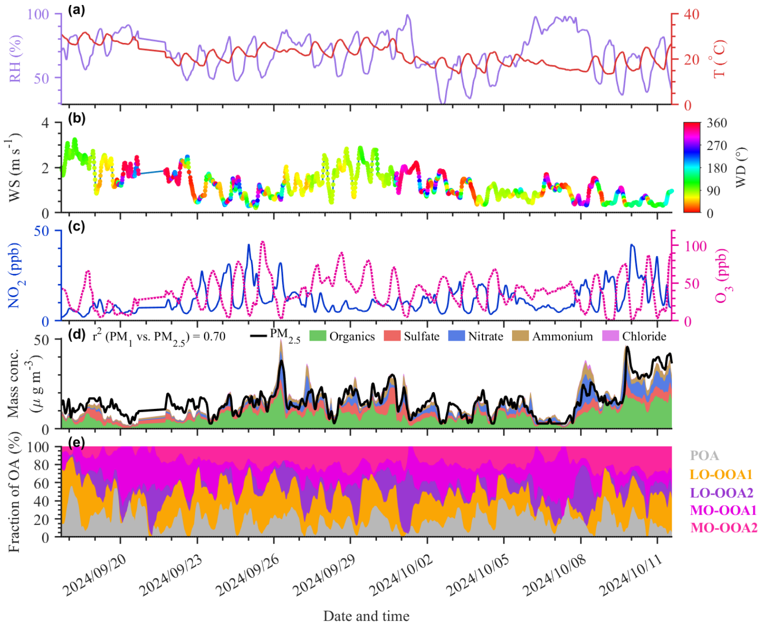

Figure 2. Overview of meteorological conditions, trace gases, and fine-particle composition during the campaign. (a) Relative humidity (RH, purple) and temperature (T, red). (b) Wind speed (WS) colored by wind direction (WD). (c) Nitrogen dioxide (NO_2, blue) and ozone (O_3, magenta). (d) $PM_{2.5}$ (black) and PM_1 chemical species: organics (Org), sulfate (SO_4^{2-}), nitrate (NO_3^-), ammonium (NH_4^+), and chloride (Cl^-); inset: correlation between PM_1 and $PM_{2.5}$. (e) Percentage contributions of PMF-resolved OA factors: POA, LO-OOA1, MO-OOA1, LO-OOA2, and MO-OOA2.

Several light pollution episodes were observed during the observation period, as indicated by the increases in fine-particle mass concentrations (Fig. 2d). PM_1 and $PM_{2.5}$ co-varied closely ($r^2 = 0.70$), with two pronounced accumulation events occurring on 26 September and 8 October. The campaign-average PM_1 concentration was 15 ± 9 µg m^{-3}, with a maximum of 50 µg m^{-3}, indicating that submicron particles dominated fine particulate mass and likely represented the major reservoir of secondary organic aerosol. In terms of chemical composition (Fig. 2d), organic aerosol (OA) was the dominant PM_1 component, contributing 50 ± 12 % on average, followed by sulfate (20 ± 8 %), nitrate (16 ± 9 %), and ammonium (12 ± 3 %), while chloride accounted for only 2 ± 1 %. This composition is characteristic of secondary aerosol-dominated conditions commonly observed at suburban sites in eastern China.

PMF applied to the AMS data resolved OA into one primary OA (POA) factor and four SOA factors (Fig. 2e). Detailed information on the AMS-PMF analysis is provided in the Supplementary Information Sect. S5. As shown in Fig. S13, SOA dominated OA composition, accounting for 80 ±11 % on average, increasing to 83 ± 10% during photochemically active daytime periods and remaining elevated (77 ± 11 %) at night. The predominance of SOA highlights the critical role of secondary formation processes in shaping aerosol composition and provides a strong foundation for subsequent molecular-level characterization and source apportionment using VIA-NO_3-CIMS measurements.

3.2 Molecular characteristics of particle-phase OOMs measured by VIA-NO_3-CIMS

3.2.1 Overall Chemical characteristic of particle-phase OOMs

During the observation period, VIA-NO_3-CIMS detected 1,695 oxygenated organic compounds (Fig. 3) with carbon numbers ranging from C_3 to C_{20}, with an overall average concentration of 1.71 µg m^{-3} based on the empirical calibration described in Sect. 2.5.2. These compounds were grouped into three classes: nitrogen-free organics

(CHO; 1,010 species; mean 1.16 µg m^{-3}), mononitrogen-containing organics (CHON; 467 species; 0.54 µg m^{-3}), and dinitrogen-containing organics ($CHON_2$; 218 species; 0.09 µg m^{-3}). By number of species, CHO dominated (60%), followed by CHON (27%) and $CHON_2$ (13%). By mass concentration, CHO contributed 69.8% of the total detected organics, with CHON and $CHON_2$ accounting for 25.2% and 4.9%, respectively. As shown in Fig. S14, the O/C–H/C distribution indicates that CHO and $CHON_x$ (x = 1, 2) primarily occupy O/C = 0.1–1.0 and H/C = 0.5–2.0, consistent with the coexistence of highly oxidized polyhydroxyl species and relatively less oxidized hydrocarbon-like derivatives, reflecting a broad range of oxidation states. Overall, CHO dominates both in species richness and signal strength, whereas nitrogen-containing organics, though less abundant, exhibit more distinctly high-oxidation signatures.

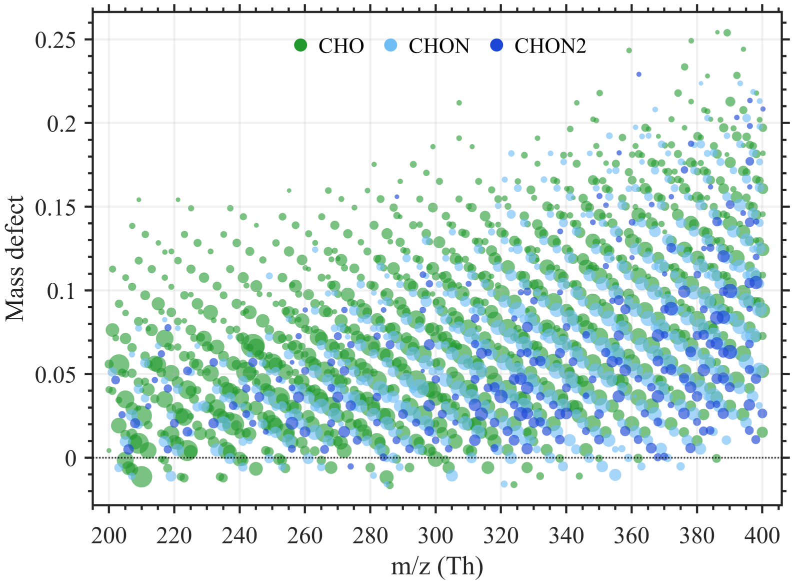

Figure 3. Mass defect versus m/z distribution of particle-phase OOMs measured by VIA-NO_3-CIMS under a fixed desorption temperature of 300 °C. Each point represents an individual compound, colored by elemental composition (CHO, CHON, and $CHON_2$), with marker area proportional to its average concentration.

A predominance of CHO species has also been reported in previous field observations employing different ionization techniques, including EESI and FIGAERO-based approaches (Ye et al., 2021; Ge et al., 2024). Although ionization selectivity can influence the relative detection efficiency of certain compound classes, particularly nitrogen-containing species, these independent observations consistently reported CHO-dominated particle-phase compositions. This consistency across measurement techniques suggests that the observed CHO dominance is unlikely due to the selectivity of nitrate chemical ionization but instead, reflects a general characteristic of ambient secondary organic aerosol.

3.2.2 Compositional differences between particle-phase and gas-phase OOMs

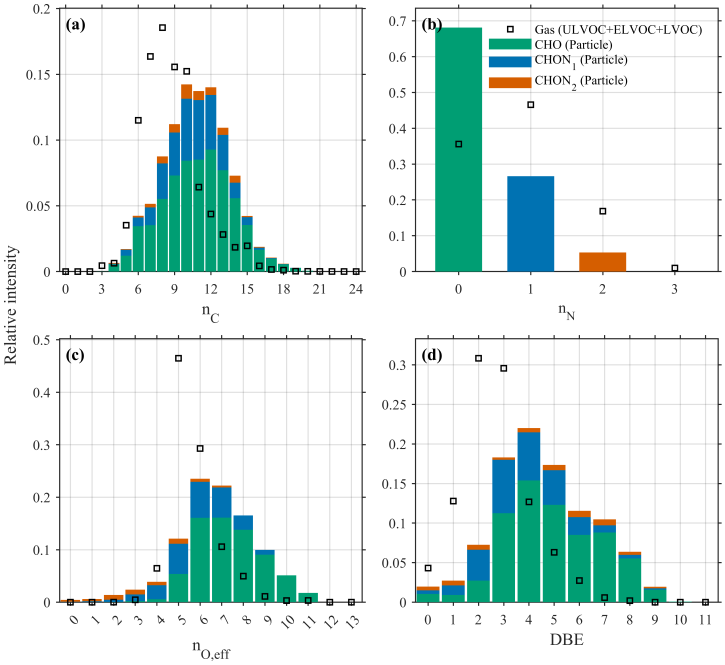

Figure 4. Comparison of elemental distributions between particle-phase OOMs (colored bars) and low-volatility gas-phase OOMs (LVOC, ELVOC, and ULVOC; black open squares) measured by VIA-NO_3-CIMS. Panels show the relative intensity distributions as a function of (a) carbon number, (b) nitrogen number, (c) effective oxygen number, and (d) double bond equivalent (DBE). The effective oxygen number is defined as Oeff=O−2N to account for oxygen atoms associated with nitrate functional groups ($–ONO_2$).

To elucidate the connection between SOA formation and OOM condensation, we compared the compositions of particle-phase OOMs with a gas-phase reference dataset. It should be noted that this reference dataset was not collected concurrently with the present measurements, but originates from a different year under comparable seasonal conditions. Therefore, the gas-phase OOM dataset is used here to provide a representative reference for examining general phase-dependent molecular characteristics, rather than for quantifying instantaneous gas–particle partitioning. The consistency of meteorological parameters and gas-phase characteristics between the two periods is discussed in Supplementary Information Sect. S7. For the analyses presented in this section, volatility was estimated using a volatility basis set (VBS) framework based on molecular composition. Specifically, the effective saturation concentration (C*) of each compound was estimated following parameterizations derived from elemental composition (Donahue et al., 2011), and compounds were subsequently assigned to volatility bins. Detailed calculation procedures and parameter settings are provided in the Supplementary Information Sect. S8.

As shown in Fig. 4, clear disparities can be observed between particle-phase OOMs and low-volatility gas-phase OOMs, including low-volatility organic compounds, extremely low-volatility organic compounds, and ultra-low-volatility organic compounds (black squares), which represent the gas-phase species most likely to contribute to SOA formation through condensation. Generally, low-volatility gas-phase OOMs are characterized by smaller carbon skeletons with $n_C \leq 10$ for major peaks, effective oxygen numbers ($n_{O,eff}$) mainly concentrated around 5–6, and DBE values generally ≤ 3. In addition, nitrogen-containing species are more abundant in the gas phase, with appreciable contributions from compounds containing at least one nitrogen atoms. These features reflect an anthropogenic dominance nature (e.g., high anthropogenic VOC and high NOx), which are consistent with the results in most studies in urban environment (Guo et al., 2022; Nie et al., 2022; Zheng et al., 2023; An et al., 2024). Comparatively, particle-phase compounds exhibit distinctly larger and more structurally complex molecular characteristics. The carbon number distribution shows a unimodal peak centered at $n_C \approx 10$ (predominantly 8–12); effective oxygen numbers are mainly in the range of 6–8; DBE values are also obviously elevated, with most particle-phase OOMs falling between 3 and 5, indicating increased structural unsaturation and functional complexity; nitrogen-containing species are substantially less abundant in the particle phase compared to the gas phase.

Although condensation of low-volatility gas-phase OOMs are known to significantly contribute to SOA mass augmentation, these systematic chemical differences clearly suggest that SOA formation involves more complicated processes than OOMs condensation, reflecting continued chemical evolution within the condensed phase. For molecules originated from gas-to-particle conversion, subsequent multiphase chemical processes, such as oxidation, oligomerization, and accretion reactions, can promote the formation of larger, more oxygenated, and lower-volatility products relative to their gas-phase precursors. Moreover, the depletion of nitrogen-containing compounds in the particle phase suggests efficient chemical losses affecting organic nitrates. Aerosol-phase hydrolysis of organic nitrates ($RONO_2$) may be a major loss pathway, converting nitrate-containing species into non-nitrate CHO compounds while releasing HNO_3 and/or forming more volatile products that repartition to the gas phase (Hu et al., 2011; Bean & Hildebrandt Ruiz, 2016; Morales et al., 2021). In addition to hydrolysis, recent laboratory and field studies have demonstrated that photolysis—both direct in the gas phase and multiphase within aerosol or aqueous media—can also represent a significant loss pathway for organic nitrates. Such photochemical degradation promotes the cleavage of the $-ONO_2$ functional group, thereby accelerating the transformation of CHON species into CHO compounds and further contributing to the depletion of particulate organic nitrates (Gen et al., 2022; González-Sánchez et al., 2023; Wang et al., 2023).

Building on the compositional comparison between particle-phase OOMs and low-volatility gas-phase OOMs described above, we further examined the volatility distributions of the complete gas-phase and particle-phase OOM datasets across the full volatility spectrum to assess whether the observed phase-dependent contrasts can be explained solely by gas–particle partitioning. As shown in Fig. 5a, the effective saturation concentration (C*) distributions differ substantially between the gas and particle phases. In the gas phase, compounds are predominantly distributed in the SVOC range, with the largest contributions occurring at C* values around 1 μg m^{-3}. The corresponding pie chart (Fig. 5b) shows that SVOC accounts for 49% of the gas-phase fraction, followed by LVOC (32%) and IVOC (11%), whereas ELVOC and ULVOC contribute only minor fractions (7% and 2%, respectively). In contrast, the particle phase is strongly enriched in low-volatility compounds. ELVOC and ULVOC contribute 35% and 30%, respectively, and LVOC represents an additional 27% of the total particle-phase fraction (Fig. 5c). Together, these three low-volatility classes constitute more than 90% of the particle-phase mass, whereas SVOC and IVOC account for only minor contributions (5% and 3%, respectively).

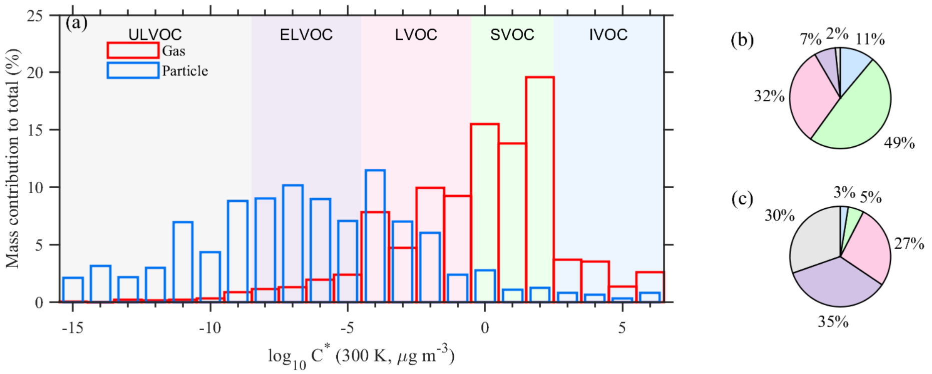

Figure 5. Volatility distributions of OOMs in the gas and particle phases. (a) Mass contribution of OOMs as a function of effective saturation concentration (C*) in the gas phase (red) and particle phase (blue). Shaded regions indicate ultra-low-volatility (ULVOC), extremely low-volatility (ELVOC), low-volatility (LVOC), semi-volatile (SVOC), and intermediate-volatility (IVOC) compounds. (b) Relative contributions of different volatility classes to total gas-phase OOMs. (c) Relative contributions of different volatility classes to total particle-phase OOMs.

Furthermore, the contribution of SVOC exhibits a clear dependence on SOA loading (Fig. S17), increasing from approximately 4.5% at low SOA levels (2–4 μg m^{-3}) to

https://doi.org/10.5194/egusphere-2026-3647
Preprint. Discussion started: 8 July 2026

about 5.3–5.5% at intermediate loadings (~8–12 μg m^{-3}), before reaching a relatively stable plateau at higher SOA concentrations. This behavior is broadly consistent with absorptive partitioning theory, whereby increasing organic aerosol mass promotes the condensation of semi-volatile compounds. However, the relatively weak increase and subsequent stabilization of the SVOC fraction suggest that gas–particle partitioning alone cannot fully explain the observed compositional evolution.

In summary, both elemental/structural characteristics and volatility distributions reveal pronounced phase-dependent differences. Gas-phase compounds are dominated by smaller, more volatile molecules, whereas particle-phase compounds are enriched in higher-carbon, more unsaturated, and substantially lower-volatility species. These systematic differences cannot be explained by equilibrium gas–particle partitioning alone, but instead highlight the critical role of particle-phase chemical processing—including accretion reactions, oligomerization, and heterogeneous oxidation—in forming and stabilizing low-volatility organic matter. Such processes contribute to the progressive transformation of initially semi-volatile vapors into lower-volatility products, thereby promoting the accumulation and persistence of secondary organic aerosol in the particle phase (Pospisilova et al., 2020; Kenseth et al., 2023; Zhang et al., 2024; Hao et al., 2025).

3.3 Molecular level source apportionment of OA

As discussed in Sect. 3.2, particle-phase organic compounds exhibit substantial contrasts in molecular characteristics relative to the gas phase, underscoring their compositional complexity and the influence of multiple precursors and atmospheric transformation pathways. Building on this overview, we performed molecular-level source apportionment using PMF applied to the VIA-NO_3-CIMS dataset to disentangle the sources and formation mechanisms of SOA. Details of the uncertainty analysis and factor selection are provided in Supplementary Information Sect. S9. The optimal solution resolved seven factors, which together explained 96% of the total OOM concentration measured by VIA–NO_3–CIMS. These factors were grouped into three major categories: (i) three biogenic-dominated SOA factors (Daytime-Biogenic-dominated-1, Daytime-Biogenic-dominated-2, and Nighttime-Biogenic-dominated); (ii) two anthropogenic-dominated SOA factors (Anthropogenic-dominated-1 and Anthropogenic-dominated-2); and (iii) two additional factors associated with regional background conditions and highly aged organic aerosol, respectively.

3.3.1 Biogenic related factors

3.3.1.1 Daytime-Biogenic-dominated-1

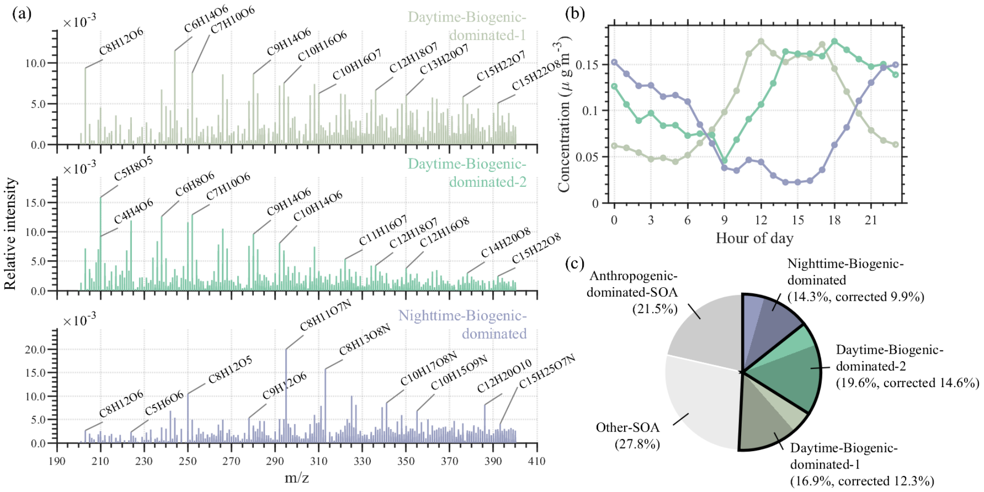

Figure 6. Mass spectral features, diurnal variations, and relative contributions of the three biogenic-related SOA factors resolved by CIMS PMF analysis. (a) Factor mass spectra, where the fingerprint molecules are marked in neutral form. (b) Average diurnal profiles. (c) Relative contributions of the three factors to total OOMs. Solid sectors indicate the original PMF contributions, while the shaded sector represents the corrected contribution of biogenic-dominated SOA.

The Daytime-Biogenic-dominated-1 factor is primarily composed of CHO compounds (~71.6%), predominantly distributed in the C_8–C_{15} range and characterized by 6–8 effective oxygen atoms (Figs. S22 and S23). As shown in Fig. 6a, the factor mass spectrum exhibits abundant oxidation products derived from biogenic VOC precursors. For example, $C_{10}H_{14}O_7$ has been widely reported as a characteristic highly oxygenated

https://doi.org/10.5194/egusphere-2026-3647
Preprint. Discussion started: 8 July 2026

monomer formed from monoterpenes such as α-pinene and limonene through initial O_3 oxidation followed by RO_2 autoxidation involving intramolecular hydrogen shifts and sequential O_2 addition (Jokinen et al., 2014; Bianchi et al., 2019). Similarly, $C_8H_{12}O_6$ (3-methyl-1,2,3-butanetricarboxylic acid, 3-MBTCA) is a well-established tracer of α-pinene SOA aging, formed through multistep gas-phase oxidation of pinic acid as well as aqueous-phase oxidation within particles or cloud water (Szmigielski et al., 2007; Müller et al., 2012). In addition, the prominent C_{15} signals (e.g., $C_{15}H_{22}O_7$ and $C_{15}H_{22}O_8$) are most plausibly derived from highly oxygenated sesquiterpene oxidation products, although contributions from $C_5 + C_{10}$ accretion reactions cannot be completely excluded (Kundu et al., 2017; Berndt et al., 2018).

From a temporal perspective, this factor exhibits a pronounced diurnal pattern, with concentrations remaining low during nighttime (~00:00–06:00 LT), increasing after sunrise, and peaking during late morning to afternoon hours (~10:00–17:00 LT), followed by a decrease toward nighttime levels (Fig. 6b). This daytime enhancement suggests a strong link to photochemically driven processes. Consistently, the factor shows moderate positive correlations with $O_3 \times$ BVOC (Fig. S25a; $r = 0.62$) indicating that its formation is associated with photochemical oxidation of BVOCs involving both OH- and O_3-initiated pathways. Together with its biogenic-dominated molecular composition, these results suggest that this factor represents secondary organic aerosol formed primarily through daytime oxidation of monoterpenes and related biogenic VOC precursors.

3.3.1.2 Daytime-Biogenic-dominated-2

The Daytime-Biogenic-dominated-2 factor is also dominated by CHO species (≈77.8%), mainly distributed in the C_5–C_{10} range with 5–7 effective oxygen atoms (Figs. S22 and S23). As shown in Fig. 6a, the molecular composition of this factor resembles that of Daytime-Biogenic-dominated-1, including contributions from monoterpene oxidation products such as $C_{10}H_{14}O_7$ and $C_8H_{12}O_6$, as well as minor contributions from larger C_{15} species. A key difference between these two factors is that larger compounds

($C \geq 10$) are substantially less abundant in Daytime-Biogenic-dominated-2, whereas smaller C_5 compounds exhibit relatively high signal intensities, including $C_5H_{8,10}O_5$ and $C_5H_{9,11}O_{6,7}N$. These compounds have been widely reported as products of multi-generation oxidation of isoprene under low-NOx conditions (Wang et al., 2018; Wennberg et al., 2018). Specifically, intermediates formed via the ISOPOOH and IEPOX pathways can undergo further OH oxidation to yield peroxy radicals, which either autoxidize (H-shift + O_2 addition) to produce compounds such as $C_5H_{8,10}O_5$, or react with NO to form $C_5H_{9,11}O_{6,7}N$ (Krechmer et al., 2015; Liu et al., 2016; D'Ambro et al., 2017). Notably, one isomer of $C_5H_8O_5$ (3-hydroxyglutaric acid) has also been identified as a tracer for α-/β-pinene photooxidation SOA (Claeys et al., 2007).

The diurnal profile provides further insight into its formation mechanism (Fig. 6b). Concentrations increase progressively during daytime and reach a maximum in the afternoon, indicating photochemically driven formation. Compared with Daytime-Biogenic-dominated-1, the peak of this factor occurs later in the day, suggesting a longer formation timescale associated with more extensive atmospheric oxidation prior to partitioning into the particle phase. This interpretation is supported by its higher average carbon oxidation state and slightly elevated O/C ratio (Fig. S24), indicating a more oxidized molecular composition. Taken together, these characteristics indicate that Daytime-Biogenic-dominated-2 represents a more aged and highly oxidized biogenic SOA factor associated primarily with multi-generation oxidation of isoprene and related biogenic VOCs.

3.3.1.3 Nighttime-Biogenic-dominated

The Nighttime-Biogenic-dominated factor exhibits the highest fraction of CHON species among all resolved factors (≈43.7%), with its composition centered on C_8–C_{10} compounds containing 5–7 effective oxygen atoms (Figs. S22 and S23). Representative compounds include $C_8H_{11}O_7N$, $C_8H_{13}O_8N$, $C_{10}H_{17}O_7N$, and $C_{10}H_{17}O_8N$ (Fig. 6a), which are widely recognized as characteristic products of nitrate radical (NO_3)-initiated oxidation of biogenic VOCs such as isoprene and monoterpenes (Lee et al., 2016; Shen

https://doi.org/10.5194/egusphere-2026-3647
Preprint. Discussion started: 8 July 2026

et al., 2021). During nighttime, isoprene and monoterpenes (e.g., α-pinene, β-pinene, limonene) react rapidly with NO_3, producing RO_2 radicals that efficiently terminate to form low-volatility multifunctional organic nitrates (Lee et al., 2016; Shen et al., 2021; Dam et al., 2022; Fouqueau et al., 2022).

As shown in Fig. 6b, the diurnal variation of this factor exhibits a pronounced nighttime enhancement: concentrations increase after ~16:00 LT, remain elevated until ~07:00 LT, and decrease to very low levels during daytime. This observation is consistent with the discussion in Sect. 3.2, highlighting the dynamic balance between formation and loss of CHON species: organic nitrates are efficiently removed by photolysis and hydrolysis during daytime, while rapid nocturnal production via NO_3 oxidation leads to transient nighttime accumulation of CHON-rich compounds.

To disentangle the controlling processes, we first examined the behavior of this factor during periods of reduced solar radiation. Cloudy conditions, characterized by substantially weakened downward solar radiation, provide a natural test of whether reduced photolytic loss alone can sustain elevated concentrations during daytime. However, as shown in Fig. S26, the relatively high concentrations during the first cloudy episode (26 September 2024) were still primarily confined to nighttime, and the factor decreased after sunrise despite persistently low solar radiation. During other cloudy periods, concentrations remained low throughout both daytime and nighttime. These observations indicate that reduced photolysis alone is insufficient to explain the observed variability, suggesting that additional controlling processes are involved.

Theoretically, NO_3 concentration can only exist at low-NO conditions. Since concurrent NO concentration is not available during this campaign, we first evaluated the relationship between O_3-NO_2-NO in the historical data at our station to understand the conditions at which low NO was encountered. As shown in Fig. S27, a high-NO and thus, suppressed-NO_3 conditions can be clearly defined at $O_3 \leq 10$ ppb and $NO_2 \geq 8$ ppb. In line with this, the majority of nighttime periods in this study fall out of such a suppressed-NO_3 condition (Fig. S26c), although some occasions of suppressed NO_3

occurred. Therefore, product $NO_2 \times O_3 \times$ BVOC is used to capture the combined influence of NO_3 formation potential and precursor abundance. As shown in Fig. S25c, the factor exhibits a acceptable positive correlation with this proxy ($r = 0.61$), suggesting that its formation is jointly controlled by both oxidant production and BVOC availability, rather than by either factor alone. Overall, we conclude that this factor is primarily linked to the NO_3-initiated oxidation of BVOCs.

3.3.1.4 Contribution of biogenic-related compounds to SOA

Although the PMF analysis identified several factors with strong biogenic characteristics, PMF-derived factors do not represent chemically pure source categories. Instead, each factor generally reflects a mixture of precursor sources and atmospheric processing. Therefore, the contribution of biogenic oxidation products to SOA cannot be directly inferred from the abundance of biogenic-dominated PMF factors alone. To provide a more quantitative constraint on the role of biogenic precursors in particle-phase SOA formation, a molecular-level classification of biogenic OOMs was further performed.

To better constrain the contribution of biogenic OOMs, a two-step identification framework was applied. First, a comprehensive list of candidate biogenic compounds was compiled based on previous laboratory and field studies, including well-established oxidation products of isoprene, monoterpenes, and sesquiterpenes formed via OH, O_3, and NO_3 oxidation pathways (Table S2). These compounds are considered to have confirmed biogenic origins and were directly classified as biogenic OOMs. Second, for compounds not included in the literature-based list, additional classification was performed using molecular-level criteria based on elemental composition and unsaturation characteristics. The molecular-level filtering criteria were generally consistent with those used for gas-phase OOMs in our previous study (Nie et al., 2022). Specifically, compounds with DBE > 4 were excluded to minimize the interference from highly unsaturated and aromatic-related species; compounds with DBE < 2 were also excluded, as these low-unsaturation species primarily represent aliphatic

https://doi.org/10.5194/egusphere-2026-3647
Preprint. Discussion started: 8 July 2026

compounds that are less characteristic of dominant BVOC oxidation products under urban atmospheric conditions. Furthermore, constraints based on effective oxygen content were applied to exclude highly oxygenated aromatic-related species ($O_{eff} > 6$ for DBE = 2). Further details on the construction of the biogenic compound list, molecular filtering criteria, and rationale for compound classification are provided in Sect. S10 of the Supplement.

Previous studies of gas-phase OOMs have suggested that biogenic species account for less than 20% of the total volatile OOM pool and therefore were estimated to contribute less than 20% of SOA through direct gas–particle condensation alone (Guo et al., 2022). In contrast, after applying the molecular-level constraints used in this study, biogenic OOMs were found to account for approximately 37% of the total observed particle-phase OOMs during the observation period (Fig. 6c). The substantially larger contribution observed in the particle phase suggests that direct condensation alone may not fully explain the incorporation of biogenic oxidation products into SOA. Instead, additional multiphase processes, such as reactive uptake and subsequent particle-phase chemical transformations, may further enhance the conversion and retention of biogenic oxidation products in the particulate phase, thereby increasing their contribution to particle-phase OOMs beyond that expected from equilibrium partitioning alone.

3.3.2 Anthropogenic related factors

3.3.2.1 Anthropogenic-dominated-1

The Anthropogenic-dominated-1 factor is primarily composed of relatively small molecules, mainly distributed in the C_5–C_8 range with 5–6 effective oxygen atoms (Fig. S23). Prominent compounds include $C_5H_8O_5$, $C_6H_{10}O_5$, and $C_6H_{12}O_6$, along with a series of nitrogen-containing aromatic oxidation products (Fig. 7a). $C_6H_{10}O_5$ and $C_6H_{12}O_6$ are commonly identified as anhydrosugars or sugar-derived compounds produced during incomplete combustion processes (e.g., biomass burning), and are widely recognized as robust tracers of combustion-related emissions (Simoneit et al.,

https://doi.org/10.5194/egusphere-2026-3647
Preprint. Discussion started: 8 July 2026

1999; Zhu et al., 2015). In addition to these primary tracers, $C_5H_8O_5$ contributes 14% of its total signal to this factor. Within the context of the biogenic-dominated factors discussed above, this compound is interpreted as a product of biogenic oxidation (e.g., from isoprene). However, previous studies have also suggested that it can be formed through aqueous-phase oxidation of levoglucosan during biomass burning, as well as oxidation of anthropogenic aromatic precursors (Kleindienst et al., 2007; Praplan et al., 2014; Zhao et al., 2014). Its co-allocation with levoglucosan-related compounds and combustion tracers within this factor suggests that, in this case, it is more likely linked to the oxidation of combustion-derived organic material.

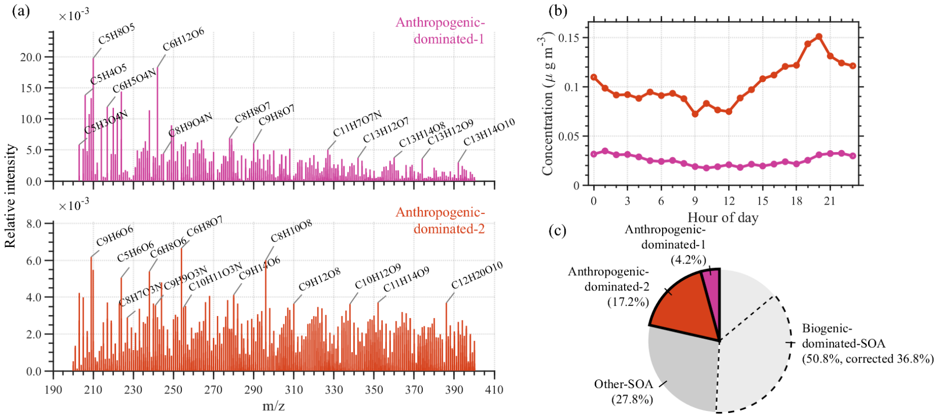

Figure 7. Mass spectral features, diurnal variations, and relative contributions of the two Anthropogenic-related SOA factors resolved by CIMS PMF analysis. (a) Factor mass spectra. The signal intensities of nitrogen-containing aromatic compounds ($C_{5\text{-}6}H_{3\text{–}5}O_4N$, $C_{5\text{-}10}H_{5\text{–}13}O_4N$, and $C_{8\text{–}17}H_{7\text{–}25}O_3N$) are multiplied by a factor of 2 for visualization. (b) Average diurnal profiles. (c) Relative contributions of the two factors to total OOMs. Solid sectors indicate the original PMF contributions, while the dashed sector represents the corrected contribution of biogenic-dominated SOA.

In addition to the compounds discussed above, this factor also contains a series of nitrogen-containing aromatic species (e.g., $C_6H_5O_4N$ and related compounds). Although their absolute signal intensities are relatively low, approximately 60–80% of

https://doi.org/10.5194/egusphere-2026-3647
Preprint. Discussion started: 8 July 2026

their total signals are attributed to this factor, indicating a strong preferential association with it. These compounds are widely recognized as nitrophenols and related nitrated aromatic species, which are primarily formed through aqueous-phase or multiphase oxidation of aromatic precursors (e.g., catechol). Previous studies have demonstrated that water-rich aerosol environments can promote the oxidation and nitration of aromatic compounds, leading to the formation of low-volatility nitrogen-containing organic species (Rana & Guzman, 2022; Shi et al., 2023; Cai et al., 2024; Kuang et al., 2025).

To further constrain the formation mechanisms of this factor, we examined its temporal behavior and correlations with key atmospheric variables. As shown in Fig. 7b, this factor does not exhibit a pronounced diurnal pattern, suggesting that it is not governed by strongly time-of-day-dependent processes. Instead, it shows a clear positive correlation with the combined proxy ALWC × AVOC (Fig. S25d, $r = 0.58$), indicating that its formation is jointly influenced by aerosol liquid water content and the availability of anthropogenic organic precursors. This dependence suggests that neither aqueous conditions nor precursor abundance alone is sufficient, and that their co-occurrence is required to facilitate efficient formation. Such behavior supports a mechanism in which water-rich particles promote the uptake and multiphase transformation of anthropogenic vapors, thereby enhancing secondary production of this factor.

Overall, Anthropogenic-dominated-1 is best interpreted as a secondary organic aerosol factor formed through aqueous-phase or multiphase processing of anthropogenic precursors, rather than a process driven by nighttime chemistry or boundary layer dynamics. Although biomass-burning-related tracers such as $C_6H_{10}O_5$ and $C_6H_{12}O_6$ are enriched in this factor, the observed correlations with ALWC × AVOC and the abundance of nitrophenols suggest that secondary processing, rather than direct emissions, dominates its formation. Despite contributing only 4.2% to total SOA (Fig. 7c), its chemical composition highlights the importance of aqueous-phase transformation of combustion-related and anthropogenic emissions in shaping SOA composition.

3.3.2.2 Anthropogenic-dominated-2

Anthropogenic-dominated-2 factor exhibits a pronounced aromatic signature, characterized by strong signals of C_8–C_{12} compounds containing 5–8 effective oxygen atoms (Fig. S23). A representative tracer is $C_9H_6O_6$ (likely trimesic acid), a multi-carboxylic product formed through multi-generation OH oxidation of alkylbenzenes followed by further functionalization and aqueous-phase aging (He et al., 2018). Additional major peaks, including $C_6H_8O_{6,7}$, $C_7H_{10}O_7$, and $C_8H_{10}O_8$, can also be attributed to highly oxygenated organic molecules produced through successive OH-driven oxidation of aromatic precursors (Garmash et al., 2020). The high oxygen content and multifunctional nature of these compounds promote efficient partitioning into the particle phase, facilitating anthropogenic SOA formation under photochemically active conditions.

Beyond the characteristic species described above, this factor also contributes substantially to a series of nitro-aromatic compounds in the $C_{8-17}H_{7-25}O_3N$ range. For example, $C_8H_7O_3N$ is likely formed through OH or NO_3 oxidation of indole, followed by NO_2 addition and subsequent functionalization or ring-opening reactions (Jiang et al., 2024). Although these nitro-aromatic species exhibit relatively low absolute signal intensities, more than 80% of their total signal is apportioned to this factor, indicating that they are overwhelmingly associated with the same oxidation regime involving anthropogenic aromatic precursors. Notably, the nitro-aromatic compounds associated with this factor are mainly characterized by formulas in the $C_xH_yO_3N$ (nitrophenols) class, whereas those enriched in Anthropogenic-dominated-1 are predominantly $C_xH_yO_4N$ (nitro-catechol) species. This systematic difference likely reflects distinct oxidation states and formation pathways. The O3N compounds in this factor are less oxygenated and therefore likely represent relatively earlier-generation nitrated products formed under active daytime oxidation conditions. In contrast, the O4N compounds in Anthropogenic-dominated-1 exhibit higher oxygen content, suggesting more extensively processed products formed through additional oxidation and/or multiphase aging facilitated by aerosol liquid water. Consistent with this molecular-level difference, bulk oxidation metrics further distinguish the two factors. Anthropogenic-dominated-1 exhibits higher average O/C ratios than Anthropogenic-dominated-2, indicating a more advanced oxidation state.

As shown in Fig. 7b, the factor exhibits a clear enhancement from late afternoon into the evening, rather than a purely nocturnal maximum. This pattern indicates that its formation is closely associated with daytime photochemical activity, with elevated concentrations persisting into the evening. Further evidence for this interpretation is provided by correlation analysis. The factor shows a clear positive relationship with the O_3 × AVOC proxy (Fig. S25e, $r = 0.57$), indicating enhanced formation under conditions characterized by both strong photochemical activity and abundant anthropogenic precursors. It should be noted that, O_3 should be interpreted as an indicator of the overall photochemical environment and oxidizing capacity, rather than as a direct oxidant of aromatic precursors. AVOCs are not efficiently oxidized by O_3 under typical atmospheric conditions; therefore, the observed dependence on O_3 reflects the co-variation of photochemical activity and reactive oxidants, rather than a direct role of O_3 itself.

In terms of quantitative contribution, Anthropogenic-dominated-2 SOA accounts for approximately 17.2% of the total SOA (Fig. 7c), highlighting its importance as a major anthropogenic SOA component in the regional aerosol. Accordingly, Anthropogenic-dominated-2 is best interpreted as a secondary organic aerosol factor formed through daytime photochemical oxidation of anthropogenic aromatic precursors. Its enrichment in highly oxygenated aromatic products and relatively less oxidized nitro-aromatic compounds underscores the important role of photochemical processing of anthropogenic emissions in shaping SOA composition under urban conditions.

3.3.3 Other factors

3.3.3.1 Regional Background factor

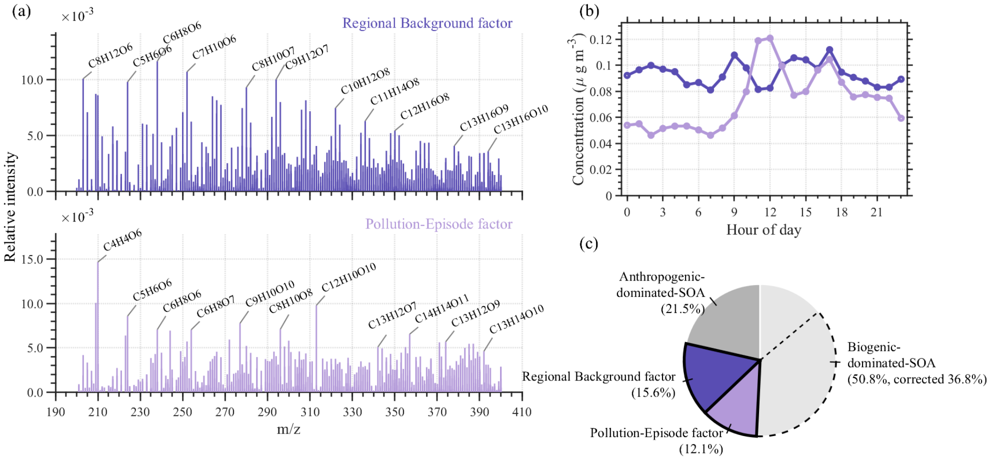

Figure 8. Mass spectral features, diurnal variations, and relative contributions of the Regional Background and Pollution-Episode factors resolved by CIMS PMF analysis. (a) Factor mass spectra. (b) Average diurnal profiles. (c) Relative contributions of the two factors to total OOMs. Solid sectors indicate the original PMF contributions, while the dashed sector represents the corrected contribution of biogenic-related SOA.

The Regional Background factor is primarily composed of C_7–C_{13} compounds containing 6–8 effective oxygen atoms, including representative species such as $C_8H_{12}O_6$, $C_9H_{10}O_6$, and $C_{12}H_{16}O_8$ (Fig. 8a). This factor exhibits the highest average carbon oxidation state ($\overline{OS}_C \approx 0.12$) among all resolved factors, together with a relatively high O:C ratio (≈0.78) and comparatively low H:C ratio (≈1.25) (Fig. S24), indicating a highly oxidized chemical composition. These values are substantially higher than those of the daytime biogenic factors ($\overline{OS}_C \approx -0.30$ to 0.02), suggesting that this factor represents organic aerosol that has undergone extensive oxidative aging.

The Regional Background factor exhibits weak diurnal variability without a clear daytime or nighttime enhancement (Fig. 8b). This pattern suggests that the factor is not primarily governed by local instantaneous formation, but instead represents an aged aerosol reservoir that has undergone extensive multi-generation oxidation, with its variability dominated by regional transport and accumulation. To assess the influence of air mass transport on this factor, we examined its potential source regions using PSCF analysis (Fig. S29a). The results reveal a broad transport corridor extending from northern China through the Yellow Sea and East China Sea regions toward the sampling site, rather than a single localized source region. Such a spatial distribution indicates a strong influence of regional-scale transport and suggests that this factor represents a widespread background aerosol component. Overall, the Regional Background factor is best interpreted as a highly oxidized and regionally distributed SOA component that reflects the accumulation of aged organic aerosol over large spatial scales rather than recent local formation.

3.3.3.2 Pollution-Episode factor

The Pollution-Episode factor is mainly composed of C_9–C_{13} compounds containing 6–9 effective oxygen atoms, including representative species such as $C_6H_8O_7$ and $C_{12}H_{10}O_{10}$ (Fig. 8a). The factor also exhibits elevated an oxidation state ($\overline{OS_C}$ ≈ 0.08; Fig. S24), indicating substantial oxidative processing. The factor shows a strong positive correlation with $PM_{2.5}$ ($r = 0.85$; Fig. S25f). However, the time series indicates that this relationship is primarily driven by several high-PM episodes, during which this factor exhibits sharp increases coinciding with $PM_{2.5}$ peaks (Fig. S30), rather than a persistent linear association.

As shown in Fig. S30, pollution episodes were classified into High-PE and Low-PE subsets according to the behavior of the Pollution-Episode factor. High-PE episodes exhibited pronounced increases in the factor concurrent with $PM_{2.5}$ peaks, whereas Low-PE episodes were characterized by elevated $PM_{2.5}$ concentrations without corresponding enhancements of the factor. To further investigate the factors controlling this contrast, the chemical and meteorological conditions associated with these two subsets were systematically compared (Fig. S31). High-PE cases are characterized by significantly elevated NO_2 and particulate nitrate, indicating enhanced NOx-related processing. In contrast, temperature, relative humidity, and ALWC are substantially

https://doi.org/10.5194/egusphere-2026-3647
Preprint. Discussion started: 8 July 2026

lower during High-PE cases, suggesting that these episodes are associated with colder and drier conditions rather than aqueous-phase processing.

To further examine the role of regional transport in shaping these characteristics, air mass analyses were conducted. The trajectory clustering analysis (Fig. S32) indicates that high-PE episodes were characterized by a substantially larger influence of northerly continental air masses originating from inland northern China, whereas marine air masses were relatively infrequent. Continental transport accounted for approximately 43% of the trajectories, with a further 23% associated with local air masses. In contrast, Low-PE episodes were primarily influenced by marine air masses, which accounted for approximately 61% of the trajectories. Overall, the Pollution-Episode factor is best interpreted as a regionally transported and chemically processed SOA component whose apparent correlation with $PM_{2.5}$ arises from episodic accumulation under specific meteorological and chemical conditions, rather than from a general contribution to bulk aerosol mass.

3.3.4 Compositional evolution of PMF factors across $PM_{2.5}$ levels

To place the behavior of individual factors in a broader atmospheric context, we further examined how the overall PMF factor composition evolves as a function of $PM_{2.5}$ concentration (Fig. 9). A clear and systematic shift in aerosol composition is observed with increasing pollution levels, reflecting changes in dominant formation regimes.

At low $PM_{2.5}$ concentrations (0–20 μg m^{-3}), the aerosol composition is dominated by freshly formed SOA, including daytime biogenic SOA and anthropogenic SOA. This feature indicates that under relatively clean conditions, aerosol formation is largely driven by local photochemical production involving both biogenic and anthropogenic precursors. As $PM_{2.5}$ concentrations increase, the relative contributions of these fresh SOA components gradually decline, accompanied by a pronounced increase in the Pollution-Episode factor. Under the most polluted conditions, the Pollution-Episode factor becomes the dominant contributor, whereas the Regional Background factor exhibits comparatively minor variations and even decreases in relative importance.

Overall, this compositional evolution reflects a transition in aerosol formation regimes, from locally driven photochemical production under clean conditions to accumulation-dominated and more extensively processed states under polluted conditions. This transition highlights the increasing importance of regional transport, atmospheric stagnation, and multi-generation chemical processing in controlling aerosol composition at high $PM_{2.5}$ levels.

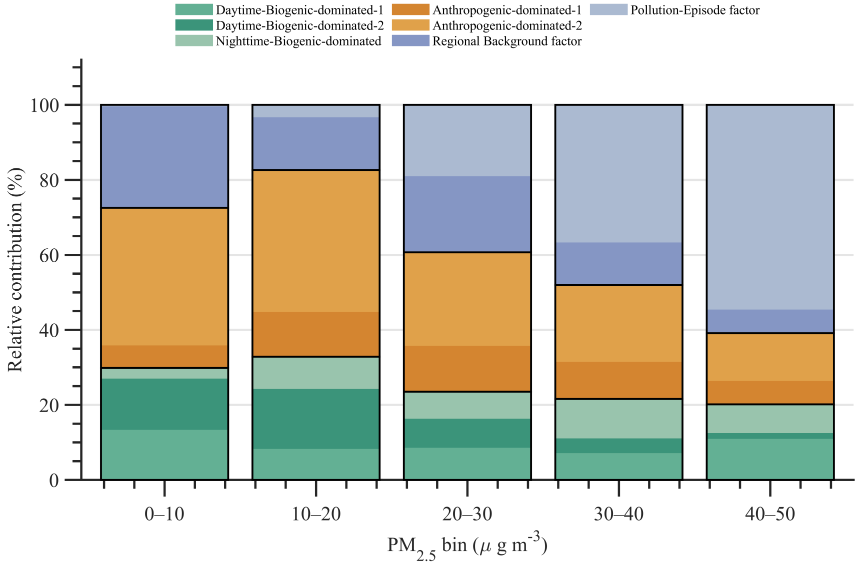

Figure 9. Constrained (reallocated) PMF factor contributions as a function of $PM_{2.5}$ concentration. Stacked bars show the relative contributions (%) of individual PMF factors within different $PM_{2.5}$ bins (0–10, 10–20, 20–30, 30–40, and 40–50 μg m^{-3}).

4. Conclusions and outlook

This study presents the first parallel field deployment of VIA-NO_3-CIMS and HR-ToF-AMS in Nanjing, eastern China, enabling molecular-level characterization of particle-phase SOA under ambient atmospheric conditions. A high-confidence dataset comprising 1,695 particle-phase OOMs (C_3–C_{20}) was established, and the summed OOM concentration showed a strong correlation with AMS-derived organic aerosol concentrations (r = 0.88), confirming that VIA-NO_3-CIMS provides quantitatively

https://doi.org/10.5194/egusphere-2026-3647
Preprint. Discussion started: 8 July 2026

meaningful constraints on particle-phase SOA variability.

At the molecular level, this study reveals systematic and fundamental differences between gas-phase and particle-phase OOMs. Particle-phase compounds are characterized by larger carbon skeletons, higher oxidation states, and substantially lower volatility, with more than 90% classified as ULVOC, ELVOC, or LVOC. These results demonstrate that particle-phase SOA composition cannot be explained solely by equilibrium gas–particle partitioning, but is strongly influenced by multiphase chemical processing. The observed enrichment of highly oxidized and low-volatility compounds provides direct field evidence that accretion reactions, oligomerization, and heterogeneous oxidation play a dominant role in transforming condensable vapors into particulate matter.

PMF analysis indicates that the molecular composition of particle-phase SOA is not governed by a single precursor source or oxidation pathway, but rather reflects the combined influence of multiple precursors, oxidation environments, and atmospheric processing. In this study, seven factors were resolved, including three biogenic-dominated factors, two anthropogenic-dominated factors, one Regional Background factor, and one Pollution-Episode factor. The biogenic factors primarily reflect the combined influence of daytime photochemical oxidation and nighttime NO_3 oxidation of BVOCs. Anthropogenic factors are associated with aromatic precursor oxidation and aqueous/multiphase processing. In contrast, the Regional Background factor represents a highly oxidized and regionally distributed SOA component, whereas the Pollution-Episode factor is associated with episodic pollution accumulation under conditions favoring regional transport and chemical processing. Moreover, SOA composition exhibits a clear transition with increasing $PM_{2.5}$, from freshly formed SOA under clean conditions to Pollution-Episode-dominated SOA under polluted conditions. This shift highlights the growing importance of regional transport, atmospheric stagnation, and multi-generation chemical processing in shaping aerosol composition during pollution episodes.

Beyond these scientific findings, this work demonstrates the unique value of VIA-NO_3-CIMS for aerosol research. Because nitrate CIMS has been widely used for gas-phase OOMs, particularly highly oxygenated organic molecules (HOMs), the use of the same ionization scheme in VIA-NO_3-CIMS provides a consistent framework for directly comparing gas-phase and particle-phase compositions. This minimizes additional bias associated with different ionization methods and offers a unique opportunity to investigate gas–particle transformation, HOM multiphase processing, and compositional evolution during particle growth. The identification of highly oxygenated and nitrogen-containing species also provides a molecular basis for understanding brown carbon formation, aerosol optical properties, and potentially health-relevant chemical characteristics.

Despite these advantages, several limitations and uncertainties remain. Nitrate chemical ionization preferentially detects highly oxygenated and low-volatility compounds, while less oxidized or more volatile species may be underrepresented. This intrinsic selectivity may introduce a systematic bias toward more oxidized compositions, leading, for example, to an overestimation of the O:C ratios of resolved OOM factors. In addition, because the VIA operates under a fixed desorption temperature, while individual compounds may exhibit different Tmax values, some species may not be fully desorbed, potentially resulting in an underestimation of their concentrations. Furthermore, compounds with lower thermal stability may undergo partial thermal decomposition during the desorption process. Together with compound-dependent desorption efficiencies, these factors may introduce systematic biases in the observed molecular composition of particle-phase organics.

Future work may further improve quantitative accuracy and molecular coverage by incorporating compound-dependent thermal desorption behavior (e.g., Tmax distributions) into the calibration framework, which could help reduce uncertainties associated with fixed-temperature operation. In addition, expanding the reagent-ion chemistry (e.g., I^-, H_3O^+, and NH_4^+) and combining VIA-NO_3-CIMS with size-resolved measurements and concurrent gas-phase observations will provide stronger constraints on gas–particle partitioning, particle growth, and multiphase aging processes. Such integrated approaches will help bridge molecular-level observations with atmospheric models and improve the representation of SOA formation and evolution in chemical transport models.

Data availability. Data are available upon request from the corresponding authors.

Competing interests. The contact author has declared that none of the authors has any competing interests.

Author contributions. CY and MC designed the study. MC conducted the field measurements, processed the data, and prepared the manuscript. CY supervised the project and contributed to data interpretation. YL, DG, JY, YL, TX, ZW, JW, YZ, ZW, ZC, BH, JW, CZ, XQ, VM, and JZ contributed to instrument operation and data interpretation. YC, QZ, ZW, ME, WN, and AD contributed to scientific discussion and manuscript revision. All authors reviewed and approved the final manuscript.

Acknowledgements. The authors thank the staff of the Station for Observing Regional Processes of the Earth System (SORPES) for their support during the field campaign. We also thank all members of the Nanjing University atmospheric chemistry group for valuable discussions and technical assistance.

Financial support. Chao Yan and Maoyu Cao acknowledge financial support from the Natural Science Foundation of China (grant no. 22327806 and 42475118). Valter

Mickwitz thanks Svenska Kultufonden (grant no. 227550) for financial support. Zhe Wang acknowledges financial support from the Hong Kong Research Grants Council (RGC) General Research Fund (Grant Nos. 16201623 and 16205724). Jian Zhao thanks Research Council of Finland (grant no. 1363283) and University of Helsinki (grant no. 70996217) for financial support.

References

An, Z., Yin, R., Zhao, X., Li, X., Li, Y., Yuan, Y., Guo, J., Zhao, Y., Li, X., Li, D., Li, Y., Wang, D., Yan, C., He, K., Worsnop, D. R., Keutsch, F. N., & Jiang, J. (2024). Molecular and seasonal characteristics of organic vapors in urban Beijing: insights from Vocus-PTR measurements. *Atmos. Chem. Phys.*, *24*(23), 13793-13810. https://doi.org/10.5194/acp-24-13793-2024

Bean, J. K., & Hildebrandt Ruiz, L. (2016). Gas–particle partitioning and hydrolysis of organic nitrates formed from the oxidation of α-pinene in environmental chamber experiments. *Atmos. Chem. Phys.*, *16*(4), 2175-2184. https://doi.org/10.5194/acp-16-2175-2016

Berndt, T., Mentler, B., Scholz, W., Fischer, L., Herrmann, H., Kulmala, M., & Hansel, A. (2018). Accretion Product Formation from Ozonolysis and OH Radical Reaction of α-Pinene: Mechanistic Insight and the Influence of Isoprene and Ethylene. *Environmental Science & Technology*, *52*(19), 11069-11077. https://doi.org/10.1021/acs.est.8b02210

Bianchi, F., Kurtén, T., Riva, M., Mohr, C., Rissanen, M. P., Roldin, P., Berndt, T., Crounse, J. D., Wennberg, P. O., Mentel, T. F., Wildt, J., Junninen, H., Jokinen, T., Kulmala, M., Worsnop, D. R., Thornton, J. A., Donahue, N., Kjaergaard, H. G., & Ehn, M. (2019). Highly Oxygenated Organic Molecules (HOM) from Gas-Phase Autoxidation Involving Peroxy Radicals: A Key Contributor to Atmospheric Aerosol. *Chemical Reviews*, *119*(6), 3472-3509. https://doi.org/10.1021/acs.chemrev.8b00395

Buchholz, A., Ylisirniö, A., Huang, W., Mohr, C., Canagaratna, M., Worsnop, D. R., Schobesberger, S., & Virtanen, A. (2020). Deconvolution of FIGAERO–CIMS thermal desorption profiles using positive matrix factorisation to identify chemical and physical processes during particle evaporation. *Atmos. Chem. Phys.*, *20*(13), 7693-7716. https://doi.org/10.5194/acp-20-7693-2020

Cai, B., Wang, Y., Yang, X., Li, Y., Zhai, J., Zeng, Y., Ye, J., Zhu, L., Fu, T.-M., & Zhang, Q. (2024). Rapid aqueous-phase dark reaction of phenols with nitrosonium ions: Novel mechanism for atmospheric nitrosation and nitration at low pH. *PNAS Nexus*, *3*(9). https://doi.org/10.1093/pnasnexus/pgae385

Canagaratna, M. R., Jayne, J. T., Jimenez, J. L., Allan, J. D., Alfarra, M. R., Zhang, Q., Onasch, T. B., Drewnick, F., Coe, H., Middlebrook, A., Delia, A., Williams, L. R., Trimborn, A. M., Northway, M. J., DeCarlo, P. F., Kolb, C. E., Davidovits, P., & Worsnop, D. R. (2007). Chemical and microphysical characterization of ambient aerosols with the aerodyne aerosol mass spectrometer. *Mass Spectrometry Reviews*, *26*(2), 185-222. https://doi.org/https://doi.org/10.1002/mas.20115

Canonaco, F., Crippa, M., Slowik, J. G., Baltensperger, U., & Prévôt, A. S. H. (2013). SoFi, an IGOR-based interface for the efficient use of the generalized multilinear engine (ME-2) for the source apportionment: ME-2 application to aerosol mass spectrometer data. *Atmos. Meas. Tech.*, *6*(12), 3649-3661. https://doi.org/10.5194/amt-6-3649-2013

Claeys, M., Szmigielski, R., Kourtchev, I., Van der Veken, P., Vermeylen, R., Maenhaut, W., Jaoui, M., Kleindienst, T. E., Lewandowski, M., Offenberg, J. H., & Edney, E. O. (2007). Hydroxydicarboxylic Acids: Markers for Secondary Organic Aerosol from the Photooxidation of α-Pinene. *Environmental Science & Technology*, *41*(5), 1628-1634. https://doi.org/10.1021/es0620181

D'Ambro, E. L., Møller, K. H., Lopez-Hilfiker, F. D., Schobesberger, S., Liu, J., Shilling, J. E., Lee, B. H., Kjaergaard, H. G., & Thornton, J. A. (2017). Isomerization of Second-Generation Isoprene Peroxy Radicals: Epoxide Formation and Implications for Secondary Organic Aerosol Yields. *Environmental Science & Technology*, *51*(9), 4978-4987. https://doi.org/10.1021/acs.est.7b00460

Dam, M., Draper, D. C., Marsavin, A., Fry, J. L., & Smith, J. N. (2022). Observations of gas-phase products from the nitrate-radical-initiated oxidation of four monoterpenes. *Atmos. Chem. Phys.*, *22*(13), 9017-9031. https://doi.org/10.5194/acp-22-9017-2022

DeCarlo, P. F., Kimmel, J. R., Trimborn, A., Northway, M. J., Jayne, J. T., Aiken, A. C., Gonin, M., Fuhrer, K., Horvath, T., Docherty, K. S., Worsnop, D. R., & Jimenez, J. L. (2006). Field-Deployable, High-Resolution, Time-of-Flight Aerosol Mass Spectrometer. *Analytical Chemistry*, *78*(24), 8281-8289. https://doi.org/10.1021/ac061249n

Ding, A. J., Nie, W., Huang, X., Chi, X. G., Sun, J. N., Kerminen, V. M., Xu, Z., Guo, W. D., Petäjä, T., Yang, X. Q., Kulmala, M., & Fu, C. B. (2016). Long-term observation of air pollution-weather/climate interactions at the SORPES station: a review and outlook. *Frontiers of Environmental Science & Engineering*, *10*(5), Article 15. https://doi.org/10.1007/s11783-016-0877-3

Donahue, N. M., Epstein, S. A., Pandis, S. N., & Robinson, A. L. (2011). A two-dimensional volatility basis set: 1. organic-aerosol mixing thermodynamics. *Atmos. Chem. Phys.*, *11*(7), 3303-3318. https://doi.org/10.5194/acp-11-3303-2011

Fouqueau, A., Cirtog, M., Cazaunau, M., Pangui, E., Doussin, J. F., & Picquet-Varrault, B. (2022). An experimental study of the reactivity of terpinolene and β-caryophyllene with the nitrate radical. *Atmos. Chem. Phys.*, *22*(10), 6411-6434. https://doi.org/10.5194/acp-22-6411-2022

Garmash, O., Rissanen, M. P., Pullinen, I., Schmitt, S., Kausiala, O., Tillmann, R., Zhao, D., Percival, C., Bannan, T. J., Priestley, M., Hallquist, Å. M., Kleist, E., Kiendler-Scharr, A., Hallquist, M., Berndt, T., McFiggans, G., Wildt, J., Mentel, T. F., & Ehn, M. (2020). Multi-generation OH oxidation as a source for highly oxygenated organic molecules from aromatics. *Atmos. Chem. Phys.*, *20*(1), 515-537. https://doi.org/10.5194/acp-20-515-2020

Ge, D., Nie, W., Liu, Y., Huang, D. D., Yan, C., Wang, J., Li, Y., Liu, C., Wang, L., Wang, J., Chi, X., & Ding, A. (2024). New Insights Into the Sources of Atmospheric Organic Aerosols in East China: A Comparison of Online Molecule-Level and Bulk Measurements. *Journal of Geophysical Research: Atmospheres*, *129*(16), e2024JD040768. https://doi.org/https://doi.org/10.1029/2024JD040768

Gen, M., Liang, Z., Zhang, R., Go, B. R., & Chan, C. K. (2022). Particulate nitrate photolysis in the atmosphere [10.1039/D1EA00087J]. *Environmental Science: Atmospheres*, *2*(2), 111-127. https://doi.org/10.1039/D1EA00087J

González-Sánchez, J. M., Brun, N., Wu, J., Ravier, S., Clément, J. L., & Monod, A. (2023). On the importance of multiphase photolysis of organic nitrates on their global atmospheric removal. *Atmos. Chem. Phys.*, *23*(10), 5851-5866. https://doi.org/10.5194/acp-23-5851-2023

Guo, Y., Yan, C., Liu, Y., Qiao, X., Zheng, F., Zhang, Y., Zhou, Y., Li, C., Fan, X., Lin, Z., Feng, Z., Zhang, Y., Zheng, P., Tian, L., Nie, W., Wang, Z., Huang, D., Daellenbach, K. R., Yao, L.,…Kulmala, M. (2022). Seasonal variation in oxygenated organic molecules in urban Beijing and their contribution to secondary organic aerosol. *Atmos. Chem. Phys.*, *22*(15), 10077-10097. https://doi.org/10.5194/acp-22-10077-2022

Häkkinen, E., Zhao, J., Graeffe, F., Fauré, N., Krechmer, J. E., Worsnop, D., Timonen, H., Ehn, M., & Kangasluoma, J. (2023). Online measurement of highly oxygenated compounds from organic aerosol. *Atmos. Meas. Tech.*, *16*(6), 1705-1721. https://doi.org/10.5194/amt-16-1705-2023

Hallquist, M., Wenger, J. C., Baltensperger, U., Rudich, Y., Simpson, D., Claeys, M., Dommen, J., Donahue, N. M., George, C., Goldstein, A. H., Hamilton, J. F., Herrmann, H., Hoffmann, T., Iinuma, Y., Jang, M., Jenkin, M. E., Jimenez, J. L., Kiendler-Scharr, A., Maenhaut, W.,…Wildt, J. (2009). The formation, properties and impact of secondary organic aerosol: current and emerging issues. *Atmos. Chem. Phys.*, *9*(14), 5155-5236. https://doi.org/10.5194/acp-9-5155-2009

Hao, P., Ye, Q., Moo, Z., DeMarsh, K., Wang, Y., Palm, B. B., Zarzana, K. J., Apel, E. C., Tyndall, G. S., Orlando, J. J., & Zhang, X. (2025). Probing the Fate of Highly Oxygenated Molecules in Atmospheric Aerosols. *Environmental Science & Technology*, *59*(28), 14540-14551. https://doi.org/10.1021/acs.est.4c07748

He, X., Huang, X. H. H., Chow, K. S., Wang, Q., Zhang, T., Wu, D., & Yu, J. Z. (2018). Abundance and Sources of Phthalic Acids, Benzene-Tricarboxylic Acids, and Phenolic Acids in PM2.5 at Urban and Suburban Sites in Southern China. *ACS Earth and Space Chemistry*, *2*(2), 147-158. https://doi.org/10.1021/acsearthspacechem.7b00131

Hu, K. S., Darer, A. I., & Elrod, M. J. (2011). Thermodynamics and kinetics of the hydrolysis of atmospherically relevant organonitrates and organosulfates. *Atmos. Chem. Phys.*, *11*(16), 8307-8320. https://doi.org/10.5194/acp-11-8307-2011

Huang, R.-J., Li, Y. J., Chen, Q., Zhang, Y., Lin, C., Chan, C. K., Yu, J. Z., de Gouw, J., Tong, S., Jiang, J., Wang, W., Ding, X., Wang, X., Ge, M., Zhou, W., Worsnop, D., Boy, M., Bilde, M., Dusek, U.,…Glasius, M. (2025). Secondary organic aerosol in urban China: A distinct chemical regime for air pollution studies. *Science*, *389*(6763), eadq2840. https://doi.org/doi:10.1126/science.adq2840

Huang, R.-J., Zhang, Y., Bozzetti, C., Ho, K.-F., Cao, J.-J., Han, Y., Daellenbach, K. R., Slowik, J. G., Platt, S. M., Canonaco, F., Zotter, P., Wolf, R., Pieber, S. M., Bruns, E. A., Crippa, M., Ciarelli, G., Piazzalunga, A., Schwikowski, M., Abbaszade, G.,…Prévôt, A. S. H. (2014). High secondary aerosol contribution to particulate pollution during haze events in China. *Nature*, *514*(7521), 218-222. https://doi.org/10.1038/nature13774

Jang, M., Czoschke, N. M., Lee, S., & Kamens, R. M. (2002). Heterogeneous Atmospheric Aerosol Production by Acid-Catalyzed Particle-Phase Reactions. *Science*, *298*(5594), 814-817. https://doi.org/doi:10.1126/science.1075798

Jiang, F., Siemens, K., Linke, C., Li, Y., Gong, Y., Leisner, T., Laskin, A., & Saathoff, H. (2024). Molecular analysis of secondary organic aerosol and brown carbon from the oxidation of indole. *Atmos. Chem. Phys.*, *24*(4), 2639-2649. https://doi.org/10.5194/acp-24-2639-2024

Jimenez, J. L., Canagaratna, M. R., Donahue, N. M., Prevot, A. S. H., Zhang, Q., Kroll, J. H., DeCarlo, P. F., Allan, J. D., Coe, H., Ng, N. L., Aiken, A. C., Docherty, K. S., Ulbrich, I. M., Grieshop, A. P., Robinson, A. L., Duplissy, J., Smith, J. D., Wilson, K. R., Lanz, V. A.,…Worsnop, D. R. (2009). Evolution of Organic Aerosols in the Atmosphere. *Science*, *326*(5959), 1525-1529. https://doi.org/doi:10.1126/science.1180353

Jokinen, T., Sipilä, M., Junninen, H., Ehn, M., Lönn, G., Hakala, J., Petäjä, T., Mauldin Iii, R. L., Kulmala, M., & Worsnop, D. R. (2012). Atmospheric sulphuric acid and neutral cluster measurements using CI-APi-TOF. *Atmos. Chem. Phys.*, *12*(9), 4117-4125. https://doi.org/10.5194/acp-12-4117-2012

Jokinen, T., Sipilä, M., Richters, S., Kerminen, V.-M., Paasonen, P., Stratmann, F., Worsnop, D., Kulmala, M., Ehn, M., Herrmann, H., & Berndt, T. (2014). Rapid Autoxidation Forms Highly Oxidized RO2 Radicals in the Atmosphere. *Angewandte Chemie International Edition*, *53*(52), 14596-14600. https://doi.org/https://doi.org/10.1002/anie.201408566

Junninen, H., Ehn, M., Petäjä, T., Luosujärvi, L., Kotiaho, T., Kostiainen, R., Rohner, U., Gonin, M., Fuhrer, K., Kulmala, M., & Worsnop, D. R. (2010). A high-resolution mass spectrometer to measure atmospheric ion composition. *Atmos. Meas. Tech.*, *3*(4), 1039-1053. https://doi.org/10.5194/amt-3-1039-2010

Kenseth, C. M., Hafeman, N. J., Rezgui, S. P., Chen, J., Huang, Y., Dalleska, N. F., Kjaergaard, H. G., Stoltz, B. M., Seinfeld, J. H., & Wennberg, P. O. (2023). Particle-phase accretion forms dimer esters in pinene secondary organic aerosol. *Science*, *382*(6672), 787-792. https://doi.org/doi:10.1126/science.adi0857

Kleindienst, T. E., Jaoui, M., Lewandowski, M., Offenberg, J. H., Lewis, C. W., Bhave, P. V., & Edney, E. O. (2007). Estimates of the contributions of biogenic and anthropogenic hydrocarbons to secondary organic aerosol at a southeastern US location. *Atmospheric Environment*, *41*(37), 8288-8300. https://doi.org/https://doi.org/10.1016/j.atmosenv.2007.06.045

Krechmer, J. E., Coggon, M. M., Massoli, P., Nguyen, T. B., Crounse, J. D., Hu, W., Day, D. A., Tyndall, G. S., Henze, D. K., Rivera-Rios, J. C., Nowak, J. B., Kimmel, J. R., Mauldin, R. L., III, Stark, H., Jayne, J. T., Sipilä, M., Junninen, H., St. Clair, J. M., Zhang, X.,…Canagaratna, M. R. (2015). Formation of Low Volatility Organic Compounds and Secondary Organic Aerosol from Isoprene Hydroxyhydroperoxide Low-NO Oxidation. *Environmental Science & Technology*, *49*(17), 10330-10339. https://doi.org/10.1021/acs.est.5b02031

Kroll, J. H., & Seinfeld, J. H. (2008). Chemistry of secondary organic aerosol: Formation and evolution of low-volatility organics in the atmosphere. *Atmospheric Environment*, *42*(16), 3593-3624. https://doi.org/https://doi.org/10.1016/j.atmosenv.2008.01.003

Kuang, Y., Luo, B., Huang, S., Liu, J., Hu, W., Peng, Y., Chen, D., Yue, D., Xu, W., Yuan, B., & Shao, M. (2025). Formation of highly absorptive secondary brown carbon through nighttime multiphase chemistry of biomass burning emissions. *Atmos. Chem. Phys.*, *25*(6), 3737-3752. https://doi.org/10.5194/acp-25-3737-2025

Kundu, S., Fisseha, R., Putman, A. L., Rahn, T. A., & Mazzoleni, L. R. (2017). Molecular formula composition of β-caryophyllene ozonolysis SOA formed in humid and dry conditions. *Atmospheric Environment*, *154*, 70-81. https://doi.org/https://doi.org/10.1016/j.atmosenv.2016.12.031

Lee, B. H., Mohr, C., Lopez-Hilfiker, F. D., Lutz, A., Hallquist, M., Lee, L., Romer, P., Cohen, R. C., Iyer, S., Kurtén, T., Hu, W., Day, D. A., Campuzano-Jost, P., Jimenez, J. L., Xu, L., Ng, N. L., Guo, H., Weber, R. J., Wild, R. J.,…Thornton, J. A. (2016). Highly functionalized organic nitrates in the southeast United States: Contribution to secondary organic aerosol and reactive nitrogen budgets. *Proceedings of the National Academy of Sciences*, *113*(6), 1516-1521. https://doi.org/doi:10.1073/pnas.1508108113

Lee, B. P., Li, Y. J., Yu, J. Z., Louie, P. K. K., & Chan, C. K. (2013). Physical and chemical characterization of ambient aerosol by HR-ToF-AMS at a suburban site in Hong Kong during springtime 2011. *Journal of Geophysical Research: Atmospheres*, *118*(15), 8625-8639. https://doi.org/https://doi.org/10.1002/jgrd.50658

Lee, C. P., Surdu, M., Bell, D. M., Dommen, J., Xiao, M., Zhou, X., Baccarini, A., Giannoukos, S., Wehrle, G., Schneider, P. A., Prevot, A. S. H., Slowik, J. G., Lamkaddam, H., Wang, D., Baltensperger, U., & El Haddad, I. (2022). High-frequency gaseous and particulate chemical characterization using extractive electrospray ionization mass spectrometry (Dual-Phase-EESI-TOF). *Atmos. Meas. Tech.*, *15*(12), 3747-3760. https://doi.org/10.5194/amt-15-3747-2022

Lelieveld, J., Evans, J. S., Fnais, M., Giannadaki, D., & Pozzer, A. (2015). The contribution of outdoor air pollution sources to premature mortality on a global scale. *Nature*, *525*(7569), 367-371. https://doi.org/10.1038/nature15371

Li, X., Cai, R., Hao, J., Smith, J. N., & Jiang, J. (2023). Online detection of airborne nanoparticle composition with mass spectrometry: Recent advances, challenges, and opportunities. *TrAC Trends in Analytical Chemistry*, *166*, 117195. https://doi.org/https://doi.org/10.1016/j.trac.2023.117195

Liu, J., D'Ambro, E. L., Lee, B. H., Lopez-Hilfiker, F. D., Zaveri, R. A., Rivera-Rios, J. C., Keutsch, F. N., Iyer, S., Kurten, T., Zhang, Z., Gold, A., Surratt, J. D., Shilling, J. E., & Thornton, J. A. (2016). Efficient Isoprene Secondary Organic Aerosol Formation from a Non-IEPOX Pathway. *Environmental Science & Technology*, *50*(18), 9872-9880. https://doi.org/10.1021/acs.est.6b01872

Liu, Y., Liu, C., Nie, W., Li, Y., Ge, D., Chen, L., Zhu, C., Wang, L., Zhang, Y., Liu, T., Qi, X., Wang, J., Huang, D., Wang, Z., Yan, C., Chi, X., & Ding, A. (2023). Exploring condensable organic vapors and their co-occurrence with PM2.5 and O3 in winter in Eastern China [10.1039/D2EA00143H]. *Environmental Science: Atmospheres*, *3*(2), 282-297. https://doi.org/10.1039/D2EA00143H

Liu, Y., Nie, W., Li, Y., Ge, D., Liu, C., Xu, Z., Chen, L., Wang, T., Wang, L., Sun, P., Qi, X., Wang, J., Xu, Z., Yuan, J., Yan, C., Zhang, Y., Huang, D., Wang, Z., Donahue, N. M.,…Ding, A. (2021). Formation of condensable organic vapors from anthropogenic and biogenic volatile organic compounds (VOCs) is strongly perturbed by NOx in eastern China. *Atmos. Chem. Phys.*, *21*(19), 14789-14814. https://doi.org/10.5194/acp-21-14789-2021

Lopez-Hilfiker, F. D., Mohr, C., Ehn, M., Rubach, F., Kleist, E., Wildt, J., Mentel, T. F., Lutz, A., Hallquist, M., Worsnop, D., & Thornton, J. A. (2014). A novel method for online analysis of gas and particle composition: description and evaluation of a Filter Inlet for Gases and AEROsols (FIGAERO). *Atmos. Meas. Tech.*, *7*(4), 983-1001. https://doi.org/10.5194/amt-7-983-2014

Lopez-Hilfiker, F. D., Pospisilova, V., Huang, W., Kalberer, M., Mohr, C., Stefenelli, G., Thornton, J. A., Baltensperger, U., Prevot, A. S. H., & Slowik, J. G. (2019). An extractive electrospray ionization time-of-flight mass spectrometer (EESI-TOF) for online measurement of atmospheric aerosol particles. *Atmos. Meas. Tech.*, *12*(9), 4867-4886. https://doi.org/10.5194/amt-12-4867-2019

Morales, A. C., Jayarathne, T., Slade, J. H., Laskin, A., & Shepson, P. B. (2021). The production and hydrolysis of organic nitrates from OH radical oxidation of β-ocimene. *Atmos. Chem. Phys.*, *21*(1), 129-145. https://doi.org/10.5194/acp-21-129-2021

Müller, L., Reinnig, M. C., Naumann, K. H., Saathoff, H., Mentel, T. F., Donahue, N. M., & Hoffmann, T. (2012). Formation of 3-methyl-1,2,3-butanetricarboxylic acid via gas phase oxidation of pinonic acid – a mass spectrometric study of SOA aging. *Atmos. Chem. Phys.*, *12*(3), 1483-1496. https://doi.org/10.5194/acp-12-1483-2012

Ng, N. L., Chhabra, P. S., Chan, A. W. H., Surratt, J. D., Kroll, J. H., Kwan, A. J., McCabe, D. C., Wennberg, P. O., Sorooshian, A., Murphy, S. M., Dalleska, N. F., Flagan, R. C., & Seinfeld, J. H. (2007). Effect of NO_x level on secondary organic aerosol (SOA) formation from the photooxidation of terpenes. *Atmos. Chem. Phys.*, *7*(19), 5159-5174. https://doi.org/10.5194/acp-7-5159-2007

Nie, W., Ding, A. J., Xie, Y. N., Xu, Z., Mao, H., Kerminen, V. M., Zheng, L. F., Qi, X. M., Huang, X., Yang, X. Q., Sun, J. N., Herrmann, E., Petäjä, T., Kulmala, M., & Fu, C. B. (2015). Influence of biomass burning plumes on HONO chemistry in eastern China. *Atmos. Chem. Phys.*, *15*(3), 1147-1159. https://doi.org/10.5194/acp-15-1147-2015

Nie, W., Yan, C., Huang, D. D., Wang, Z., Liu, Y., Qiao, X., Guo, Y., Tian, L., Zheng, P., Xu, Z., Li, Y., Xu, Z., Qi, X., Sun, P., Wang, J., Zheng, F., Li, X., Yin, R., Dallenbach, K. R.,…Ding, A. (2022). Secondary organic aerosol formed by condensing anthropogenic vapours over China's megacities. *Nature Geoscience*, *15*(4), 255-261. https://doi.org/10.1038/s41561-022-00922-5

Paatero, P., & Tapper, U. (1994). Positive matrix factorization: A non-negative factor model with optimal utilization of error estimates of data values. *Environmetrics*, *5*(2), 111-126. https://doi.org/https://doi.org/10.1002/env.3170050203

Pospisilova, V., Lopez-Hilfiker, F. D., Bell, D. M., El Haddad, I., Mohr, C., Huang, W., Heikkinen, L., Xiao, M., Dommen, J., Prevot, A. S. H., Baltensperger, U., & Slowik, J. G. (2020). On the fate of oxygenated organic molecules in atmospheric aerosol particles. *Science Advances*, *6*(11), eaax8922. https://doi.org/doi:10.1126/sciadv.aax8922

Praplan, A. P., Hegyi-Gaeggeler, K., Barmet, P., Pfaffenberger, L., Dommen, J., & Baltensperger, U. (2014). Online measurements of water-soluble organic acids in the gas and aerosol phase from the photooxidation of 1,3,5-trimethylbenzene. *Atmos. Chem. Phys.*, *14*(16), 8665-8677. https://doi.org/10.5194/acp-14-8665-2014

Pye, H. O. T., Nenes, A., Alexander, B., Ault, A. P., Barth, M. C., Clegg, S. L., Collett Jr, J. L., Fahey, K. M., Hennigan, C. J., Herrmann, H., Kanakidou, M., Kelly, J. T., Ku, I. T., McNeill, V. F., Riemer, N., Schaefer, T., Shi, G., Tilgner, A., Walker, J. T.,…Zuend, A. (2020). The acidity of atmospheric particles and clouds. *Atmos. Chem. Phys.*, *20*(8), 4809-4888. https://doi.org/10.5194/acp-20-4809-2020

Rana, M. S., & Guzman, M. I. (2022). Oxidation of Catechols at the Air–Water Interface by Nitrate Radicals. *Environmental Science & Technology*, *56*(22), 15437-15448. https://doi.org/10.1021/acs.est.2c05640

Shen, H., Zhao, D., Pullinen, I., Kang, S., Vereecken, L., Fuchs, H., Acir, I.-H., Tillmann, R., Rohrer, F., Wildt, J., Kiendler-Scharr, A., Wahner, A., & Mentel, T. F. (2021). Highly Oxygenated Organic Nitrates Formed from NO3 Radical-Initiated Oxidation of β-Pinene. *Environmental Science & Technology*, *55*(23), 15658-15671. https://doi.org/10.1021/acs.est.1c03978

Shi, X., Qiu, X., Li, A., Jiang, X., Wei, G., Zheng, Y., Chen, Q., Chen, S., Hu, M., Rudich, Y., & Zhu, T. (2023). Polar Nitrated Aromatic Compounds in Urban Fine Particulate Matter: A Focus on Formation via an Aqueous-Phase Radical Mechanism. *Environmental Science & Technology*, *57*(13), 5160-5168. https://doi.org/10.1021/acs.est.2c07324

Shrivastava, M., Cappa, C. D., Fan, J., Goldstein, A. H., Guenther, A. B., Jimenez, J. L., Kuang, C., Laskin, A., Martin, S. T., Ng, N. L., Petaja, T., Pierce, J. R., Rasch, P. J., Roldin, P., Seinfeld, J. H., Shilling, J., Smith, J. N., Thornton, J. A., Volkamer, R.,…Zhang, Q. (2017). Recent advances in understanding secondary organic aerosol: Implications for global climate forcing. *Reviews of Geophysics*, *55*(2), 509-559. https://doi.org/https://doi.org/10.1002/2016RG000540

Simoneit, B. R. T., Schauer, J. J., Nolte, C. G., Oros, D. R., Elias, V. O., Fraser, M. P., Rogge, W. F., & Cass, G. R. (1999). Levoglucosan, a tracer for cellulose in biomass burning and atmospheric particles. *Atmospheric Environment*, *33*(2), 173-182. https://doi.org/https://doi.org/10.1016/S1352-2310(98)00145-9

Stark, H., Yatavelli, R. L. N., Thompson, S. L., Kang, H., Krechmer, J. E., Kimmel, J. R., Palm, B. B., Hu, W., Hayes, P. L., Day, D. A., Campuzano-Jost, P., Canagaratna, M. R., Jayne, J. T., Worsnop, D. R., & Jimenez, J. L. (2017). Impact of Thermal Decomposition on Thermal Desorption Instruments: Advantage of Thermogram Analysis for Quantifying Volatility Distributions of Organic Species. *Environmental Science & Technology*, *51*(15), 8491-8500. https://doi.org/10.1021/acs.est.7b00160

Sun, Y., Luo, H., Li, Y., Zhou, W., Xu, W., Fu, P., & Zhao, D. (2025). Atmospheric organic aerosols: online molecular characterization and environmental impacts. *npj Climate and Atmospheric Science*, *8*(1), 305. https://doi.org/10.1038/s41612-025-01199-2

Sun, Y. L., Wang, Z. F., Fu, P. Q., Yang, T., Jiang, Q., Dong, H. B., Li, J., & Jia, J. J. (2013). Aerosol composition, sources and processes during wintertime in Beijing, China. *Atmos. Chem. Phys.*, *13*(9), 4577-4592. https://doi.org/10.5194/acp-13-4577-2013

Szmigielski, R., Surratt, J. D., Gómez-González, Y., Van der Veken, P., Kourtchev, I., Vermeylen, R., Blockhuys, F., Jaoui, M., Kleindienst, T. E., Lewandowski, M., Offenberg, J. H., Edney, E. O., Seinfeld, J. H., Maenhaut, W., & Claeys, M. (2007). 3-methyl-1,2,3-butanetricarboxylic acid: An atmospheric tracer for terpene secondary organic aerosol. *Geophysical Research Letters*, *34*(24). https://doi.org/https://doi.org/10.1029/2007GL031338

Voliotis, A., Wang, Y., Shao, Y., Du, M., Bannan, T. J., Percival, C. J., Pandis, S. N., Alfarra, M. R., & McFiggans, G. (2021). Exploring the composition and volatility of secondary organic aerosols in mixed anthropogenic and biogenic precursor systems. *Atmos. Chem. Phys.*, *21*(18), 14251-14273. https://doi.org/10.5194/acp-21-14251-2021

Wang, J., Ge, X., Chen, Y., Shen, Y., Zhang, Q., Sun, Y., Xu, J., Ge, S., Yu, H., & Chen, M. (2016). Highly time-resolved urban aerosol characteristics during springtime in Yangtze River Delta, China: insights from soot particle aerosol mass spectrometry. *Atmos. Chem. Phys.*, *16*(14), 9109-9127. https://doi.org/10.5194/acp-16-9109-2016

Wang, Y., Takeuchi, M., Wang, S., Nizkorodov, S. A., France, S., Eris, G., & Ng, N. L. (2023). Photolysis of Gas-Phase Atmospherically Relevant Monoterpene-Derived Organic Nitrates. *The Journal of Physical Chemistry A*, *127*(4), 987-999. https://doi.org/10.1021/acs.jpca.2c04307

Yang, L. H., Takeuchi, M., Chen, Y., & Ng, N. L. (2021). Characterization of thermal decomposition of oxygenated organic compounds in FIGAERO-CIMS. *Aerosol Science and Technology*, *55*(12), 1321-1342. https://doi.org/10.1080/02786826.2021.1945529

Ye, C., Yuan, B., Lin, Y., Wang, Z., Hu, W., Li, T., Chen, W., Wu, C., Wang, C., Huang, S., Qi, J., Wang, B., Wang, C., Song, W., Wang, X., Zheng, E., Krechmer, J. E., Ye, P., Zhang, Z.,…Shao, M. (2021). Chemical characterization of oxygenated organic compounds in the gas phase and

https://doi.org/10.5194/egusphere-2026-3647
Preprint. Discussion started: 8 July 2026

particle phase using iodide CIMS with FIGAERO in urban air. *Atmos. Chem. Phys.*, *21*(11), 8455-8478. https://doi.org/10.5194/acp-21-8455-2021

Yin, J., Liu, Y., Nie, W., Yan, C., Zha, Q., Li, Y., Ge, D., Liu, C., Zhu, C., Chi, X., & Ding, A. (2025). Unveiling the formation of atmospheric oxygenated organic molecules under anthropogenic–biogenic interactions: insights from binned positive matrix factorization on multi-subrange mass spectra. *Atmos. Chem. Phys.*, *25*(20), 13279-13297. https://doi.org/10.5194/acp-25-13279-2025

Yuan, Y., Chen, X., Cai, R., Li, X., Li, Y., Yin, R., Li, D., Yan, C., Liu, Y., He, K., Kulmala, M., & Jiang, J. (2024). Resolving Atmospheric Oxygenated Organic Molecules in Urban Beijing Using Online Ultrahigh-Resolution Chemical Ionization Mass Spectrometry. *Environmental Science & Technology*, *58*(40), 17777-17785. https://doi.org/10.1021/acs.est.4c04214

Zhang, W., Issa, K., Tang, T., & Zhang, H. (2024). Role of Hydroperoxyl Radicals in Heterogeneous Oxidation of Oxygenated Organic Aerosols. *Environmental Science & Technology*, *58*(10), 4727-4736. https://doi.org/10.1021/acs.est.3c09024

Zhang, X., McVay, R. C., Huang, D. D., Dalleska, N. F., Aumont, B., Flagan, R. C., & Seinfeld, J. H. (2015). Formation and evolution of molecular products in α-pinene secondary organic aerosol. *Proceedings of the National Academy of Sciences*, *112*(46), 14168-14173. https://doi.org/doi:10.1073/pnas.1517742112

Zhang, Y., Peräkylä, O., Yan, C., Heikkinen, L., Äijälä, M., Daellenbach, K. R., Zha, Q., Riva, M., Garmash, O., Junninen, H., Paatero, P., Worsnop, D., & Ehn, M. (2019). A novel approach for simple statistical analysis of high-resolution mass spectra. *Atmos. Meas. Tech.*, *12*(7), 3761-3776. https://doi.org/10.5194/amt-12-3761-2019

Zhao, J., Mickwitz, V., Luo, Y., Häkkinen, E., Graeffe, F., Zhang, J., Timonen, H., Canagaratna, M., Krechmer, J. E., Zhang, Q., Kulmala, M., Kangasluoma, J., Worsnop, D., & Ehn, M. (2024). Characterization of the Vaporization Inlet for Aerosols (VIA) for online measurements of particulate highly oxygenated organic molecules (HOMs). *Atmos. Meas. Tech.*, *17*(5), 1527-1543. https://doi.org/10.5194/amt-17-1527-2024

Zhao, R., Kenseth, C. M., Huang, Y., Dalleska, N. F., Kuang, X. M., Chen, J., Paulson, S. E., & Seinfeld, J. H. (2018). Rapid Aqueous-Phase Hydrolysis of Ester Hydroperoxides Arising from Criegee Intermediates and Organic Acids. *The Journal of Physical Chemistry A*, *122*(23), 5190-5201. https://doi.org/10.1021/acs.jpca.8b02195

Zhao, R., Mungall, E. L., Lee, A. K. Y., Aljawhary, D., & Abbatt, J. P. D. (2014). Aqueous-phase photooxidation of levoglucosan – a mechanistic study using aerosol time-of-flight chemical ionization mass spectrometry (Aerosol ToF-CIMS). *Atmos. Chem. Phys.*, *14*(18), 9695-9706. https://doi.org/10.5194/acp-14-9695-2014

Zheng, P., Chen, Y., Wang, Z., Liu, Y., Pu, W., Yu, C., Xia, M., Xu, Y., Guo, J., Guo, Y., Tian, L., Qiao, X., Huang, D. D., Yan, C., Nie, W., Worsnop, D. R., Lee, S., & Wang, T. (2023). Molecular Characterization of Oxygenated Organic Molecules and Their Dominating Roles in Particle Growth in Hong Kong. *Environmental Science & Technology*, *57*(20), 7764-7776. https://doi.org/10.1021/acs.est.2c09252

Zhu, C., Kawamura, K., & Kunwar, B. (2015). Effect of biomass burning over the western North Pacific Rim: wintertime maxima of anhydrosugars in ambient aerosols from Okinawa. *Atmos. Chem. Phys.*, *15*(4), 1959-1973. https://doi.org/10.5194/acp-15-1959-2015